

Hydrological Sciences Journal

ISSN: (Print) (Online) Journal homepage: https://www.tandfonline.com/loi/thsj20

Comparing actual evapotranspiration estimations by METRIC to in-situ water balance measurements over an irrigated field in Turkey

Mahmut Cetin, Omar Alsenjar, Hakan Aksu, Muhammet Said Golpinar & Mehmet Ali Akgul

To cite this article: Mahmut Cetin, Omar Alsenjar, Hakan Aksu, Muhammet Said Golpinar & Mehmet Ali Akgul (2023) Comparing actual evapotranspiration estimations by METRIC to in-situ water balance measurements over an irrigated field in Turkey, Hydrological Sciences Journal, 68:8, 1162-1183, DOI: 10.1080/02626667.2023.2198649

To link to this article: https://doi.org/10.1080/02626667.2023.2198649

Published online: 19 May 2023.

Submit your article to this journal

Article views: 306

View related articles

View Crossmark data

Full Terms & Conditions of access and use can be found at
https://www.tandfonline.com/action/journalInformation?journalCode=thsj20

HYDROLOGICAL SCIENCES JOURNAL
2023, VOL. 68, NO. 8, 1162–1183
https://doi.org/10.1080/02626667.2023.2198649

Check for updates

Comparing actual evapotranspiration estimations by METRIC to in-situ water balance measurements over an irrigated field in Turkey

Mahmut Cetin [a], Omar Alsenjar [a], Hakan Aksu [b], Muhammet Said Golpinar [a] and Mehmet Ali Akgul [c]

[a]Department of Agricultural Structures and Irrigation, Cukurova University, Adana, Turkey; [b]Department of Meteorological Engineering, Samsun University, Samsun, Turkey; [c]Department of Information Technologies, the Sixth Regional Directorate of State Hydraulic Works, Adana, Turkey

ABSTRACT

Estimating actual evapotranspiration (ETa) rates in large-scale irrigation schemes is of great importance to improve water use efficiency. Crop types can be determined by employing remote sensing techniques coupled with ground truth data. This study aimed to: (a) conduct a water balance study by making in-situ water balance measurements, (b) derive cropping pattern maps, (c) acquire crop evapotranspiration (ETc), (d) generate fully distributed ETa maps, and (e) compare ETa estimations with ETc and in-situ water balance. Landsat 7 and 8 satellite data, and meteorological data were used to estimate ETa in the Eastern Mediterranean Region of Turkey in the 2021 hydrological year. Crop types were classified using Sentinel 2A–2B satellite images. The change in catchment storage was +67.08 mm with a 3.34% water balance closure error. The correlation between ETa and ETc for irrigated wheat, potato, lettuce, corn-1, peanut-1, soybean-2, and citrus was significant in the growing season.

ARTICLE HISTORY
Received 13 September 2022
Accepted 27 February 2023

EDITOR
A. Castellarin

ASSOCIATE EDITOR
A. Petroselli

KEYWORDS
water requirements; irrigation water management; remote sensing; irrigation schemes; artificial neural networks (ANN)

1 Introduction

Although crop evapotranspiration (ETc), along with precipitation, is one of the most crucial elements of the water cycle in irrigation schemes, it cannot be directly quantified in large irrigation schemes. Accurate estimation of ETc is still a challenging issue, especially in water-scarce areas. Today, the negative impacts of climate change and the growing population, particularly in the world's semi-arid regions, are putting pressure on water supply systems. Hirich *et al.* (2020) pointed out that the current level of climate change, which is linked to high evapotranspiration and global warming, has already aggravated the food and water security situation in these regions. In this regard, accurate assessment of ETc allows water authorities, water managers, farmers, and others to make better use of precious water resources.

Evapotranspiration (ET) is typically defined as the transfer of water to the atmosphere from the land surface through evaporation by soil with water surfaces and transpiration by plants (Allen *et al.* 2007a, Gowda *et al.* 2008). Because in-situ point measurements are only representative of small regions, estimating precise ET values over large areas has been a challenging issue. To estimate actual evapotranspiration (ETa) or crop evapotranspiration, many direct and indirect evapotranspiration estimation methods have been developed and put into practice for a long time. These methods are lysimeter, water balance, eddy covariance, pan evaporation, atmometer, Bowen ratio–energy balance system (BREBS), scintillometer, empirical methods, and remote sensing (RS), among others. In recent years, RS techniques have been used to estimate ETa in both large irrigation schemes and hydrological basins (Allen *et al.* 2011a, Aksu and Arikan 2017). RS techniques provide end users with a cost-effective approach to monitoring ETa at a regional scale (Mokhtari *et al.* 2021).

RS-based evapotranspiration estimation techniques can be grouped into four categories: empirical direct methods, residual methods of the energy budget, deterministic methods, and vegetation index methods (Courault *et al.* 2005). Nowadays, energy balance approaches such as Surface Energy Balance Algorithm for Land (SEBAL) (Bastiaanssen *et al.* 1998a, 1998b), Mapping Evapotranspiration at high Resolution and with Internalized Calibration (METRIC) (Allen *et al.* 2007a, 2007b), and Surface Energy Balance System (SEBS) (Su 2002) are the most frequently used RS-based methods and can be categorized as land surface temperature-based approaches (Biggs *et al.* 2016).

The satellite-based METRIC model has been used to estimate ETa in many places around the world for sustainable agricultural water management, hydrological modelling, and the establishment of water rights, among other uses (see Allen *et al.* 2007b, 2011a, 2011b, Trezza *et al.* 2013, Aksu and Arikan 2017, Madugundu *et al.* 2017, Numata *et al.* 2017, Tasumi 2019, Jaafar and Ahmad 2020). METRIC is an image processing model employed to estimate ETa as a residual of the surface energy balance equation by using data obtained from satellite images, and hence, instant data acquired from nearby meteorological stations. The METRIC model can be applied in both flat and mountainous terrains (Allen *et al.* 2013). For example, the METRIC model was applied by using RS data, i.e., Moderate

CONTACT Omar Alsenjar omarsenjar@yahoo.com Department of Agricultural Structures and Irrigation, Cukurova University, Adana, Turkey
© 2023 IAHS

Resolution Imaging Spectroradiometer (MODIS) data, over the Büyük Menderes basin in Turkey (Aksu and Arikan 2017), Landsat 5 and 7 over an almond orchard in California (He *et al.* 2017), and Landsat 8 over an irrigated field in Saudi Arabia (Madugundu *et al.* 2017) and over both irrigated and rain-fed agricultural fields in the western Urmia Lake Basin in Iran (Tasumi 2019). Allen *et al.* (2007b) summarized the results of 19 studies that include verification of METRIC and/or SEBAL. The 19 studies have an average 4.5% disagreement with in-situ point measurements of ETa obtained via ground-based methods. Allen *et al.* (2007a) reported errors ranging from 3% to 20% between ground-based measurements and METRIC model estimations. Moreover, the METRIC model estimations were found to be consistent with the Class A-pan data (Aksu and Arikan 2017), eddy covariance method results (Madugundu *et al.* 2017), and Penman-Monteith reference ETo (Tasumi 2019). The METRIC model can produce gridded actual evapotranspiration maps by using RS images with high resolution. Consequently, these ETa maps may be used in quantifying water balance components at the catchment scale. To this end, the spatial resolution of Landsat satellite imagery is high enough to monitor the spatiotemporal variations of ET in the field parcels. For example, Anderson *et al.* (2012) addressed the fact that field sizes are smaller than 0.1 ha (30 m × 30 m) in many developing countries. Turkey has similarly small field sizes in its irrigation schemes. For this reason, we used Landsat 7 and Landsat 8 data in this research.

The validation process for RS-based ET estimations is the most challenging issue. To overcome difficulties, a two-step approach is generally adopted (Steduto 2000, Cetin 2020b): (a) reference evapotranspiration (ETo) estimation, and (b) multiplication of ETo by crop coefficient (Kc). In this regard, determination of the cropping pattern is of great importance. "Cropping pattern" refers to the proportion of area under different types of crops at different locations or parcels in time. It also indicates the time and spatial arrangement or sequence of crops and/or fallow in a particular land area. Mapping spatial coverage of crops grown in an area using RS techniques is the most efficient and cost-effective method for estimating the actual evapotranspiration. However, the selection of satellite imagery for crop classification is based on many factors, such as the availability of images, diversity level in crop types, and the extensiveness of the study area (Zheng *et al.* 2015). Literature reviews have shown that Sentinel-2 has been widely used in precision agriculture for crop monitoring applications (Sonobe *et al.* 2017, Belgiu and Csillik 2018, Whyte *et al.* 2018). For example, Defourny *et al.* (2019) classified five major crop types and non-agriculture areas in different countries (Ukraine, Mali, and South Africa) and five local sites distributed around the world using the Sentinel-2 and Landsat 8 data. The overall accuracy of the classification was higher than 80% for all sites except one. For their part, Jiang *et al.* (2020) produced a high-resolution map of the main crop types for three large regions located in China (2–3 crop types per region), achieving an average overall accuracy of 94%.

In this study, crop types were classified with the Artificial Neural Network (ANN) algorithm in the ENVI (Environment for Visualizing Images) software, using the Neural Net Classification module under the Supervised Classification with Sentinel-2 and ground truth data; then, cropping pattern maps were generated. Additionally, estimation of ETa was done using a RS-based energy balance technique, i.e., the METRIC model. We used the estimated ETa values to perform monthly and annual water balance calculations together with precipitation, net drainage, and irrigation diversions measured daily at the gauging stations using automatic water level recorders. The novelty of this work is illustrated by the scarcity of similar studies such as RS studies on evapotranspiration estimation, water balance calculations based on in-situ hydrologic observations, and crop pattern classification in the study area. As such, it should be considered the first attempt to classify crop types and determine the annual catchment storage changes in the root zone based on actual evapotranspiration estimates by the METRIC model coupled with in-situ irrigation and drainage flow rate measurements in a large-scale irrigation district in the Eastern Mediterranean Region of Turkey.

The primary objectives of this study were to: (a) conduct a water balance study by making in-situ water balance measurements in a large-scale irrigation district; (b) derive cropping pattern maps using Sentinel-2 satellite images, classified by the ANN procedure coupled with a myriad of ground truth data, for the winter and summer seasons; (c) acquire daily crop evapotranspiration (ETc) series for the study site following the FAO-56 method, i.e., the "two-step approach"; (d) estimate daily actual evapotranspiration (ETa) from the satellite-based RS METRIC model and generate fully distributed daily ETa maps in a sub-catchment of the Lower Seyhan Plain (LSP) in the Eastern Mediterranean region of Turkey; (e) compare ETa estimations with the ETc method for some crops; and (f) use the ETa estimations in water balance calculations.

2 Material and methods

2.1 Study area

This study was conducted in a catchment with large-scale irrigation, i.e., Akarsu Irrigation District (hereafter, AID) with a total area of 9495 ha. The AID is substantially a flat terrain, situated in the Lower Seyhan Plain (LSP) in the southeastern Mediterranean region of Turkey (Fig. 1). The AID is located between 36°57′32″ and 36°50′43″N latitudes and between 35°40′22″ and 35°28′42″E longitudes. The Mediterranean climate, characterized by a hot and dry summer season and a warm and rainy winter season, fully dominates the LSP. The annual average, minimum and maximum air temperatures in the AID are 18.9, 9.0, and 31.0°C, respectively. The annual mean precipitation of the basin is 649.5 mm (Cetin *et al.* 2020a). Temperature, evaporation, transpiration, and relative humidity reach their maximum values in the irrigation season (IS; i.e., in July and August), whereas the minimum values are observed in the rainy season, i.e., particularly in the winter months (December, January, and February), in the Eastern Mediterranean Region of Turkey.

Seyhan Plain has great agricultural potential for the Turkish economy; most lands of the plain are considered irrigated areas. It hosts various crop types, such as corn, cereals, citrus, cotton, soybean, watermelon, onion, pasture, and vegetables. The dominant Mediterranean climate makes it possible to grow multiple

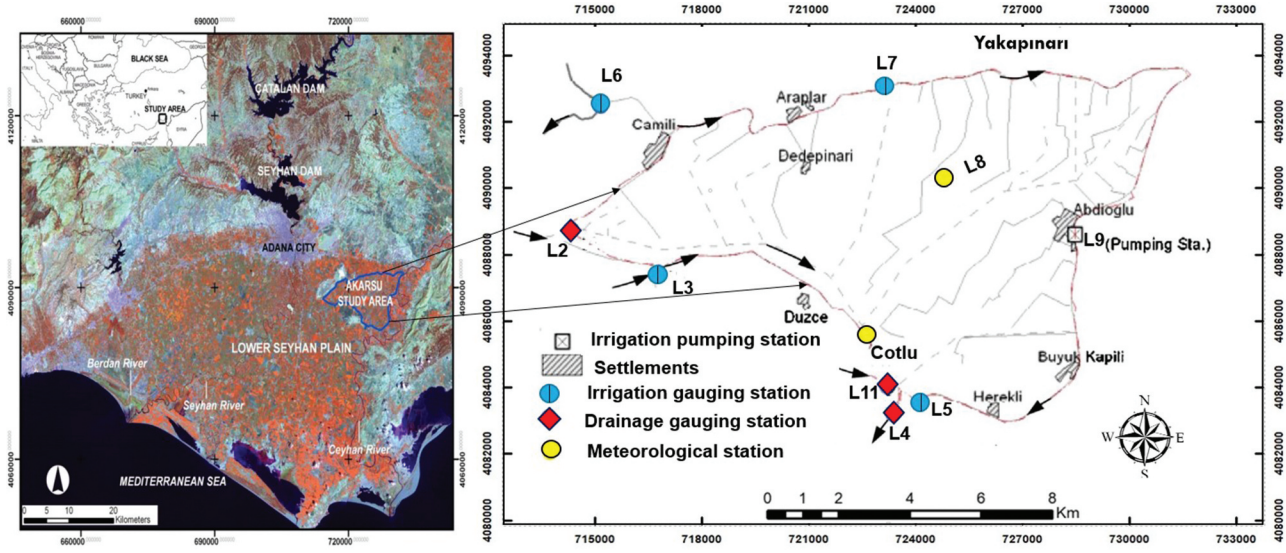


Figure 1. The study area, located in the Eastern Mediterranean region of Turkey. Dotted lines, solid (continuous) lines and arrows represent the drainage and irrigation canals, and water flow directions, respectively, in the district. L3, L6, L7 and L9 are irrigation water input locations; L5 is an irrigation water output location; L2 and L11 are drainage water input locations, and L4 is a drainage output located at the outlet of the catchment. Meteorological stations are located at L8 and Cotlu.

crops in a year. As such, major winter crops are wheat, potato, onion, and lettuce, while summer crops are corn, cotton, soybean, groundnut, and watermelon (Ozcan *et al.* 2003). The winter season in Turkey typically falls between the first of December and the end of February. The summer season, in contrast, runs from the first of June to the end of August. Figure 2 shows types of crops commonly grown in the area, along with their growing periods and the lengths of crop growth stages (i.e., initial, development, mid-season, and late season).

2.2 Reference evapotranspiration (ETo) calculation

Hourly and daily climate data (temperature, wind speed, solar radiation, precipitation) obtained from the two meteorological stations located in the AID (Fig. 1) were utilized in the study to calculate ETo: (a) L8 meteorological station, and (b) Cotlu meteorological station. The reference ETo values were computed using weather datasets and by applying the FAO Penman-Monteith method (Equation (1)) (Allen *et al.* 1998). Equation (1) was developed for short grass; the albedo and aerodynamic resistance were 0.23 and 70 sm^{-1}, respectively.

$$ETo = \frac{0.408\Delta(R_n - G) + \gamma\frac{900}{T+273}u_2(e_s - e_a)}{\Delta + \gamma(1 + 0.34u_2)} \quad (1)$$

where ETo is the reference evapotranspiration (mm day^{-1}), R_n is the net radiation at the crop surface (MJ m^{-2} day^{-1}), G is the soil heat flux density (MJ m^{-2} day^{-1}), T is the mean daily air temperature at 2 m height (°C), u_2 is the wind speed at 2 m height (m s^{-1}), e_s is the saturation vapor pressure (kPa), e_a is the actual vapor pressure (kPa), $e_s - e_a$ is the saturation vapor pressure deficit (kPa), Δ slope (kPa°C^{-1}) is the vapor pressure curve, and γ is the psychrometric constant (kPa°C^{-1}).

2.3 Satellite images for estimating actual evapotranspiration

Landsat Satellite images were used for the ETa estimations. Landsat 7 (ETM^+) and Landsat 8 Thermal Infrared Sensor and Operational Land Imager (OLI) (path 175, row 34) with 30 m

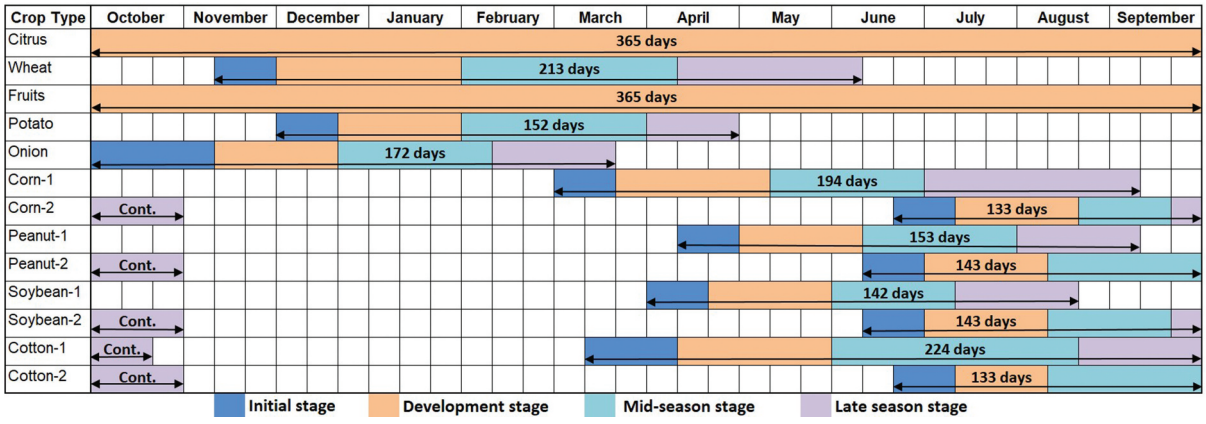


Figure 2. Common crop types grown in the study area, their growing periods, and the "length of crop growth stages" (initial, development, mid-season, and late season).

Table 1. Availability of Landsat 7 and Landsat 8 scene information in the 2021 water year: names of scenes, acquisition dates, and overpass time.

Image #	Day of the year (DOY)	Landsat scene	Satellite	Cloud cover (%)	Acquisition dates	Overpass time (am, local)
1	260	LC81750342020260LGN00	Landsat 8	1	16 September 2020	11:15:56.5028510
2	300	LE71750342020300SG100	Landsat 7	8	26 October 2020	10:38:56.1154274
3	316	LE71750342020316NPA00	Landsat 7	3	11 November 2020	10:37:51.0228172
4	364	LE71750342020364NPA00	Landsat 7	1	29 December 2020	10:34:21.8153233
5	22	LC81750342021022LGN00	Landsat 8	9	22 January 2021	11:15:49.9861710
6	54	LC81750342021054LGN00	Landsat 8	7	23 February 2021	11:15:43.2139690
7	79	LE71750342021078SG100	Landsat 7	5	19 March 2021	10:28:24.8443048
8	118	LC81750342021118LGN00	Landsat 8	8	28 April 2021	11:15:15.8809360
9	134	LC81750342021134LGN00	Landsat 8	1	14 May 2021	11:15:15.9098560
10	158	LE71750342021158SG100	Landsat 7	1	07 June 2021	10:21:43.6865663
11	182	LC81750342021182LGN00	Landsat 8	4	01 July 2021	11:15:35.1871370
12	190	LE71750342021190SG100	Landsat 7	3	09 July 2021	10:19:04.5579664
13	198	LC81750342021198LGN00	Landsat 8	5	17 July 2021	11:15:36.9021800
14	214	LC81750342021214LGN00	Landsat 8	0	02 August 2021	11:15:45.3409259
15	230	LC81750342021230LGN00	Landsat 8	2	18 August 2021	11:15:51.0643500
16	262	LC81750342021262LGN00	Landsat 8	9	19 September 2021	11:15:59.0216650
17	278	LC81750342021278LGN00	Landsat 8	1	05 October 2021	11:16:04.4435930

by 30 m spatial resolution were downloaded from the USGS website (http://earthexplorer.usgs.gov), shown in Table 1. The Landsat images are typically available every 16 days for satellite scenes. For the two growing seasons in the 2021 water year, 17 Landsat 7 and Landsat 8 satellite images were used in this research (Table 1) and cloud cover was less than 10% for all processed images. Quality control checks (gaps in the data, outliers, constant values, jumps, etc.) were applied to ensure the quality and integrity of the meteorological data. Table 2 shows the average daily meteorological data at the satellite overpass day, i.e., daily data, including wind speed, air temperature, relative humidity, and solar radiation.

2.4 Crop evapotranspiration (ETc) estimation

In this study, the performance of the METRIC model was compared to independently estimated ETc values acquired by FAO-56 as in Tasumi (2019). Therefore, crop evapotranspiration (ETc) was estimated by multiplying reference evapotranspiration (ETo) by a crop coefficient Kc determined according to the crop type and growing stages, i.e., a two-step approach (Allen *et al.* 1998, Steduto 2000, Cetin 2020b), as follows:

$$ETc = Kc\ ETo \quad (2)$$

where ETc is crop evapotranspiration (mm day^{-1}) and Kc is the crop coefficient (local Kc values for different crop growth stages were taken from the available literature by TAGEM-DSI (2017)). Spatio-temporal changes in Kc values were included in the study to represent the crop's status at different growth stages, i.e., initial crop development, mid-season (second and third stages), and late season, for crops that are common in the winter and summer seasons in Turkey's LSP. ETo (mm day^{-1}) is defined and calculated using the FAO Penman-Monteith approach given by Allen *et al.* (1998).

2.5 In-situ observations of water balance components and forming a water balance

The water year in the Mediterranean countries as well as in Turkey covers the period between 1 October of one year and 30 September of the following year. To form a water balance at the irrigation district level, inflows (irrigation diversions, irrigation return flows (IRFs) – i.e., drainage flows generated by upstream agricultural lands – and precipitation) to the AID and outflows (irrigation flows from the district to downstream, IRFs) were observed at flow rate gauging stations shown in Fig. 1.

Table 2. Average daily meteorological data during the satellite overpass day.

Day of the year (DOY)	Wind speed (m s^{-1})	Air temperature (°C)	Relative humidity (%)	Solar radiation (MJ m^{-2} day^{-1})
260	0.57	28.60	73.13	18.34
300	0.78	26.00	44.00	13.43
316	0.40	18.77	60.71	11.98
364	0.61	11.33	52.95	9.80
22	0.80	7.35	62.95	12.00
54	1.30	11.60	49.35	17.00
79	1.80	12.25	66.05	20.40
118	1.30	20.85	72.90	23.60
134	1.20	22.20	64.90	26.80
158	1.64	23.18	66.47	28.08
182	1.74	28.71	72.14	25.85
190	1.56	29.02	71.27	25.02
198	1.32	29.64	70.17	24.23
214	1.31	30.5	66.43	23.45
230	1.35	28.31	70.91	23.19
262	1.18	25.22	67.74	16.23
278	1.36	21.30	46.94	15.32

As shown in Fig. 1, L8 and Cotlu automatic meteorological stations provided the climatic variables (temperature, wind speed, solar radiation, and relative humidity) for ET calculation, viz. ETo and ETa, as well as the precipitation data for forming a water balance work. A tipping bucket raingauge with 0.2 mm precision was used in precipitation data observation. Net irrigation and net drainage flow rates (in- and outflows) were measured all the time using electronic limnigraph devices, with a measurement precision of ±1.0 mm, installed on the inputs and outputs of irrigation and drainage canals – L3, L6, L7, and L9 (L9 is a pumping station to divert irrigation water from the Ceyhan River to the study area in the peak IS) are installed on irrigation inputs, L5 on irrigation output; L2 and L11 on drainage inputs and L4 on drainage output – as shown in Fig. 1. Limnigraphs were set up to measure the water depths at the canal cross-sections, and then the discharge values were obtained using rating curves developed specifically for channel sections located in Fig. 1. Observed water depths were recorded on an hourly basis by averaging six readings at 10-minute intervals in an hour. Firstly, hourly discharges ($m^3\ s^{-1}$) were calculated, and then flow rates were accumulated as explained by Cetin *et al.* (2020a) to acquire daily water amounts ($m^3\ day^{-1}$) for the 2021 water year.

The basic formula for water balance calculations (Loucks *et al.* 2005, Cetin *et al.* 2020a) is given in Equation (3):

$$P + (I_{in} - I_{out}) - (Q_{out} - Q_{in}) - ET = \pm\Delta S \quad (3)$$

where P is precipitation, I_{in} is irrigation inflows (L3, L6, L7, L9 in Fig. 1), Q_{in} is drainage inflows (incoming from outside areas; L2 and L11 in Fig. 1), ET is crop evapotranspiration (either ETa or ETc, based on its availability), I_{out} is irrigation outflows (discharging from the main irrigation canal, L5 in Fig. 1), Q_{out} is drainage outflows at the outlet of the AID (L4 in Fig. 1), and ΔS is the change in the catchment storage including error term. All inputs and outputs in the water balance method are in millimetres. Because the water budget terms (P, net irrigation and net drainage, and ΔS) are derived from ground truth observations, some measurement and processing errors in these datasets are inherently expected (Tapley *et al.* 2004a, Swenson and Wahr 2006, Daly *et al.* 2008, Landerer and Swenson 2012, Ibrikci *et al.* 2015). In this manner, the ΔS term was considered the closure error of the water balance work since there was no precise way of measuring catchment storage in our case. Consequently, the magnitude of closure error in the water balance (Ibrikci *et al.* 2015) was quantified monthly as follows:

$$\text{Error } \Delta = 200 * \frac{(\text{Total inputs} - \text{Total outputs})}{(\text{Total inputs} + \text{total outputs})} \quad (4)$$

2.6 Crop type processing

Crop classification produces pivotal data on crop types at the regional scale and thus on cropping patterns. Figure 3(a) illustrates the general procedure for crop type determination in an irrigation catchment. In general terms, crop type determination consists of three steps: (1) data inputs; (2) pre-processing and training; and (3) final classification. To originate the precise insights, we united data from Sentinel-2 images with a 10-m resolution and ground truth data acquired by surveying various croplands or fields, i.e., farm parcels, in both winter and summer seasons, then applied an artificial neural network (ANN) to find the field boundaries and classify different types of crops.

2.6.1 Pre-processing of Sentinel-2 images and ground truth data

In the first step, we downloaded Sentinel-2A-2B images, which are available at https://scihub.copernicus.eu/dhus/#/home and described in Table 3. The Sentinel-2A-2B images were processed for atmospheric and radiometric correction using the ENVI software. To achieve high accuracy in classification studies, the normalized difference vegetation index (NDVI) was calculated as follows:

$$NDVI = \frac{(NIR_{band8} - Red_{band4})}{(NIR_{band8} + Red_{band4})} \quad (5)$$

where NIR_{band} and Red_{band} are the corrected spectral radiance in the near-infrared and red bands, respectively (Rouse *et al.* 1974). The resulting NDVI values were included in the study to increase the accuracy of the ANN classification.

Ground truth data should be acquired by making field surveys in different croplands at different times (Karnez 2010), i.e., visiting fields in the winter season (i.e., from December to February), at the beginning of the IS (i.e., in March and April) and during the most intense period of irrigation in the summer season (i.e., in July and August). However, in our study, two field campaigns were carried out for collecting ground truth crop data: (a) during the winter/spring season of 2021 (on 1–7 March 2021), (b) during the peak IS in the summer season (on 12–13 July 2021). During field campaigns, the parcels were visited and existing plant species or land use types in the parcels, including empty fields, were noted on the map. In addition to noting the plant species, the coordinates of the parcels visited were also determined with a handheld GPS [UTM, Datum = WGS84], and duly recorded. After completion of fieldwork, parcel-based spatial data were transferred to the computer environment by using the ArcGIS program to generate cropping pattern maps.

2.6.2 Crop classification by ANN model

In the second step, where the crop-type classification was implemented in the ENVI program using the Neural Net Classification module under Supervised Classification, the logistic activation method was used. This research uses a multi-layered feedforward neural network containing an input layer consisting of 10 nodes in the winter season and 16 nodes in the summer season as a region of interest (ROI), three hidden layers and one node as an output layer, as shown in Fig. 3(a). The connections between the input layers and the three hidden layers take different weights, and the weights are finally trained based on the required output, in our case the classified map (Novelli *et al.* 2016, Zalnezhad *et al.* 2022). The ANN technology requires the feedforward and back-propagation processes for allowing the network to be trained.

The estimated NDVI image was added as a band to the RS data in order to obtain high classification accuracy, and the image to be analysed was transformed into a five-band image

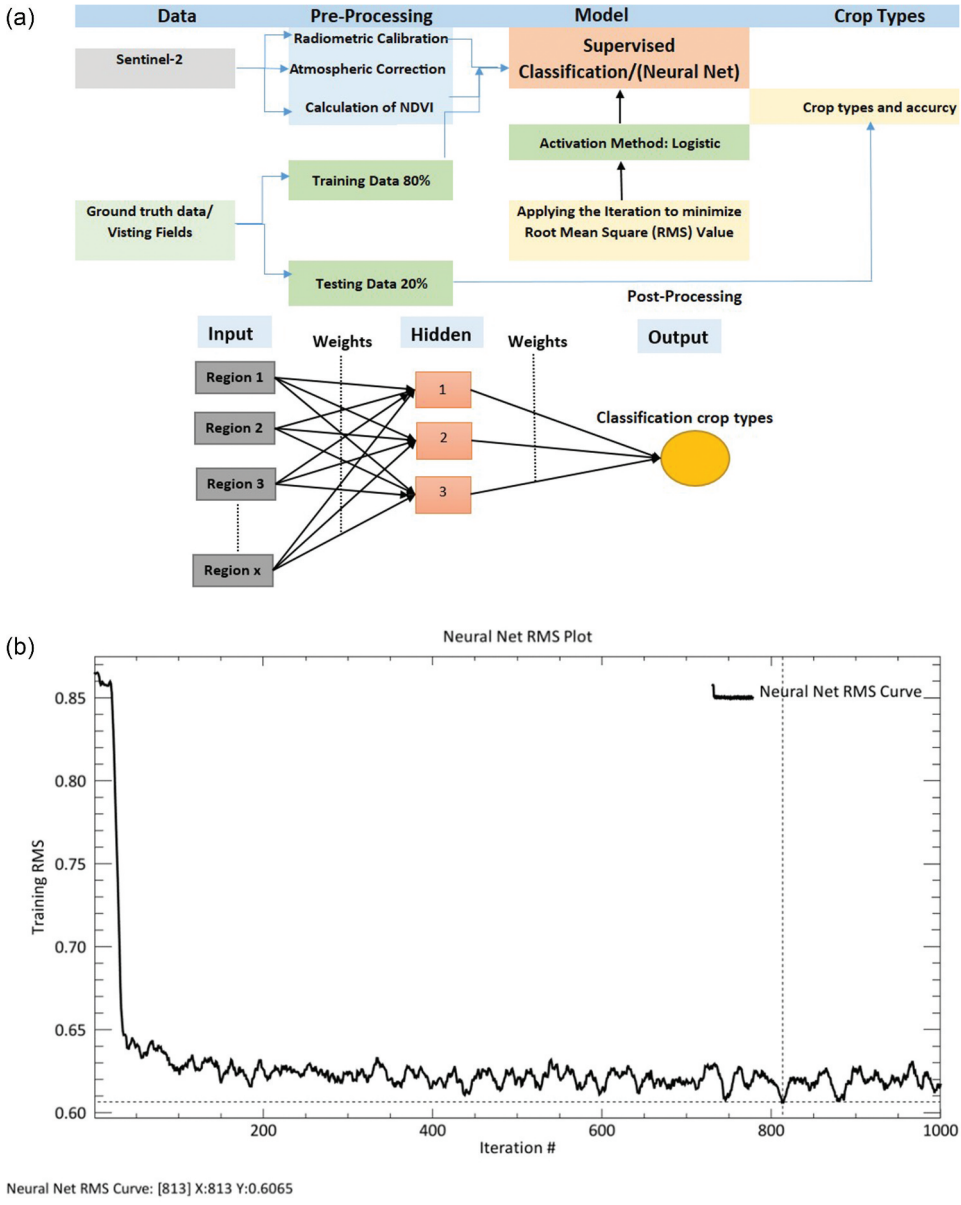


Figure 3. (a) Image processing steps for determination of crop types grown in the irrigation district in summer and winter seasons, along with their input data, pre-processing, and models; (b) plot comparing training RMS and the iteration value in the winter season of 2021.

Table 3. Sentinel satellite image names and dates used for summer and winter plant pattern recognition in the research area.

Image name	DOY
S2B_MSIL2A_20200413T082559_N0214_R021_T36SYF_20200413T115830	104
S2B_MSIL2A_20200702T082609_N0214_R021_T36SYF_20200702T122946	184
S2A_MSIL1C_20200806T082611_N0209_R021_T36SYF_20200806T100018	219
S2B_MSIL2A_20210319T082639_N0214_R021_T36SYF_20210319T112002	78
S2B_MSIL2A_20210329T082559_N0214_R021_T36SYF_20210329T111602	88
S2A_MSIL2A_20210413T082601_N0300_R021_T36SYF_20210413T105415	103
S2B_MSIL2A_20210627T082559_N0300_R021_T36SYF_20210627T112602	178
S2A_MSIL2A_20210811T082601_N0301_R021_T36SYF_20210811T114551	223

(red, green, blue, NIR and NDVI). The ground truth data converted to ROI format and the five-band images were introduced into the ENVI program as part of the neural network classification method for the crop types. The iteration value was obtained against the neural net (NN) root mean square (RMS) curve and was acquired separately in the winter and summer classification map of 2021. Then, the iteration value was trained to produce the lowest RMS used in the classification; Fig. 3(b) shows an example in the winter season.

Post-processing is required to verify the cropping pattern map estimated by the ANN algorithm using ground truth data. For this reason, the confusion matrix, as the output of ANN,

was computed using 20% of ground truth data for each crop type (Boken *et al.* 2004, Mahlayeye *et al.* 2022) in this research.

2.7 METRIC model

The METRIC model was applied to estimate ETa for each pixel, each crop type, and the whole study area Equation (6) using Landsat satellite imagery, based on Allen *et al.* (2007a) and using a Water Package in the R program (Olmedo *et al.* 2016). In this context, latent heat flux (LE) is calculated as the following:

$$LE = R_n - G - H \tag{6}$$

where R_n is the net radiation flux at the surface, G is the soil heat flux, and H is the sensible heat flux. Rn, G and H are in the same units (commonly in W m^{-2}).

Net radiation (R_n) is calculated using surface reflectance and surface temperature (Ts) derived from satellite imagery. R_n is the difference between incoming shortwave radiation and outgoing longwave radiation, calculated as follows:

$$R_n = R_s\downarrow - \alpha R_s\downarrow + R_L\downarrow - R_L\uparrow - (1 - \varepsilon_o)R_L\downarrow \tag{7}$$

where $R_s\downarrow$ is the incoming shortwave radiation (solar radiation), α is the surface albedo (dimensionless), and $R_L\downarrow$ is the incoming longwave radiation, $R_L\uparrow$ is the outgoing longwave radiation, and ε_o is the surface thermal emissivity (dimensionless).

Soil heat flux (G) is defined as the rate of heat storage in the soil and vegetation due to conduction (Allen *et al.* 2007a). G was computed using the following equations proposed by Tasumi (2003):

$$\frac{G}{R_n} = 0.05 + 0.18e^{-0.521\ LAI}(LAI \geq 0.5) \tag{8}$$

$$\frac{G}{R_n} = 1.80(T_s - 273.16)/R_n + 0.084(LAI < 0.5) \tag{9}$$

where Ts stands for surface temperature (K) and is determined from a satellite image. Equation (9) suggests that when the leaf area index (LAI) is less than 0.5, the G/R_n ratio increases with higher rates of Ts and decreases with increasing LAI.

Sensible heat flux (H) was determined using the aerodynamic-based heat transfer equation as follows:

$$H = \frac{\rho_{air} C_p dT}{r_{ah}} \tag{10}$$

where ρ_{air} is the air density (kg m^{-3}), C_p is the air-specific heat (1004 J kg^{-1} K^{-1}), dT is the temperature difference between two heights z_1 (0.1 m) and z_2 (2 m), and r_{ah} is the aerodynamic resistance to heat transfer (s m^{-1}).

Based on LE values, the instantaneous values of ETa were computed for each pixel as follows:

$$ET_{inst} = \frac{3600\ LE}{\lambda\ \rho w} \tag{11}$$

where ET_{inst} is the instantaneous ETa at the satellite overpass (mm h^{-1}); 3600 is the conversion factor from seconds to hours; LE is the latent heat flux (W m^{-2}) consumed by ET; ρw is the density of water = 1000 kg m^{-3}; and λ is the latent heat of vaporization (J kg^{-1}), which is computed as follows:

$$\lambda = \left(2.501 - 0.00236(T_s - 273.15)10^6\right) \tag{12}$$

Daily values of ET (ET_{24}) (mm day^{-1}) for each pixel were calculated as follows:

$$ET_{24} = ET_rF\ ET_r24 \tag{13}$$

where ET_rF is the reference ET fraction; ET_r24 is the cumulative short-grass reference evapotranspiration, i.e., ETo, for the day (mm day^{-1}); and ET_{24} is the actual evapotranspiration, i.e., METRIC ETa, for the entire 24-hour period (mm day^{-1}). Values for ET_rF are computed based on ET_{inst} for each pixel, and ET_r was obtained from local weather data as follows:

$$ET_rF = \frac{ET_{inst}}{ET_r} \tag{14}$$

Accumulated ETa values for a given month or for a season t days in length are calculated as in Equation (15) using ETrF values interpolated for the days between satellite images and ETr computed from ground-based meteorological data. Annual ETa is then obtained by aggregating daily values.

Monthly ET, on aggregate, is calculated as follows:

$$ET_m = \sum_{i=1}^{m}[ET_rF_iET_r24_i] \tag{15}$$

where ET_m stands for accumulative ET for a month ending on day *m*, ET_rF_i is the interpolated ET_rF for day *i*, and ET_r24_i is the 24-h ET_r for day *i*. All are in units of mm day^{-1}.

After estimating daily ETa for each pixel and classifying crop types by RS over the study area, it becomes easy to estimate daily ETa for each crop type and the whole study area, as follows:

$$ETa_{cropi} = \frac{\sum_{i=1}^{n}[ETa_iA_i]}{\sum_{i=1}^{n}A_i} \tag{16}$$

An average ETa for the whole study area can be calculated as:

$$ETa_{study\ area} = \frac{\sum_{i=1}^{n}\left[ETa_{cropi}A_i\right]}{\sum_{i=1}^{n}A_i} \tag{17}$$

where ETa_{cropi} is actual evapotranspiration for each crop in each pixel for a day *i* (mm day^{-1}), A_i is the area of crop in each pixel (m^2) for crop *i*, $ETa_{study\ area}$ is the mean value of ETa for the whole study area for a day *i* (mm day^{-1}), and *i* is the crop type.

We can obtain cumulative ETa for each crop type and the whole study area for any period (e.g. month, season, or year) by applying the procedure in Equation (15).

2.8 Statistical comparisons

In this study, the difference between ETa-METRIC and ETc was statistically assessed using a simple linear regression approach (*ETc = a + b ETa-METRIC*) for some crop types (wheat, potato, lettuce, corn-1, peanut-1, soybean-2, and citrus). Other statistical evaluations such as mean bias error (MBE in Equation (18)), root mean square error (RMSE in

Equation (19)), and coefficient of determination (R^2 in Equation (20)) were used.

$$MBE = \frac{1}{n}\sum_{i=1}^{n}(x_i - y_i) \quad (18)$$

$$RMSE = \sqrt{\frac{\sum_{i=1}^{n}(x_i - y_i)^2}{n}} \quad (19)$$

$$R^2 = \left(\frac{\sum_{i=1}^{n}(x_i - \overline{x})(y_i - \overline{y})}{\sqrt{\sum_{i=1}^{n}(x_i - \overline{x})^2}\sqrt{\sum_{i=1}^{n}(y_i - \overline{y})^2}} \right)^2 \quad (20)$$

where *x* and *y* stand for actual evapotranspiration (*ETa-METRIC*) and independently estimated ET (Tasumi 2019) following the FAO-56, also known as the "*two-step procedure*" (*ETc*), respectively.

3 Results and discussion

3.1 Precipitation and reference evapotranspiration (ETo)

Given the major impact of meteorological conditions on ET, a thorough examination of climate conditions is required to make a sound assessment. The rainfall amounts and other meteorological observations related to the climate conditions were analysed, on a daily time scale, during the 2021 water year. Meteorological data indicated that climatic conditions over the study area were hot and dry in summer and cool in the winter. Therefore, as shown in Fig. 4, ETo ranged between 0.67 mm day^{-1} (minimum value on 14 January 2021 = DOY 14) and 8.08 mm day^{-1} (maximum value on 28 July 2021 = DOY 209). In addition, Fig. 4 shows the variation of monthly ETo values, ranging from 43 mm (all-time low in both December and January) to 189 mm (all-time high in July). The annual total ETo was about 1308 mm for the 2021 hydrological year. Annual ETo values were found to be in good agreement with the findings by Ibrikci *et al.* (2015). As shown in Fig. 4, variability in daily precipitation (P) and ETo is more distinctive than in their monthly counterparts. As can be seen from the results acquired in 2021, the daily mean reference evapotranspiration and its standard deviation were around 3.59 mm day^{-1}, and 1.80 mm day^{-1}, respectively. The annual total precipitation (476.6 mm) of the 2021 water year was lower by 183 mm (almost 28% less than normal) compared to the annual mean precipitation of the basin (Cetin *et al.* 2020a). Based on the meteorological observations, most of the rainfalls occurred in the winter season (382 mm), whereas rainfall events rarely occurred in the summer season; this is a typical feature of the Mediterranean climate.

3.2 Crop type classification and crop distribution mapping

As shown in Fig. 5, ground truth data were illustrated using the spatial datasets acquired during the field campaigns in the winter and summer seasons. In the winter season, a total of 1316 parcels were visited and crops grown on those parcels were noted, while the number was 1469 parcels in the summer of 2021. Since the citrus planting areas were determined within the scope of another study, the sampling density was deliberately kept low in these areas, as shown in Fig. 5.

Furthermore, Fig. 6 shows the results of the crop classification in both the winter and summer periods. Supervised classification of crop types by the ANN algorithm helped us generate cropping pattern maps of high accuracy. The overall accuracy, on average, was about 92% for winter and summer crop distribution maps. As shown in Fig. 6, citrus-planted areas were dominant (≈39% in winter and ≈43% in summer, indicating an increase) in the eastern parts of the study area throughout the year. However, a significant part of the land (≈39%) is empty, i.e., bare soil, in winter, kept in reserve for the

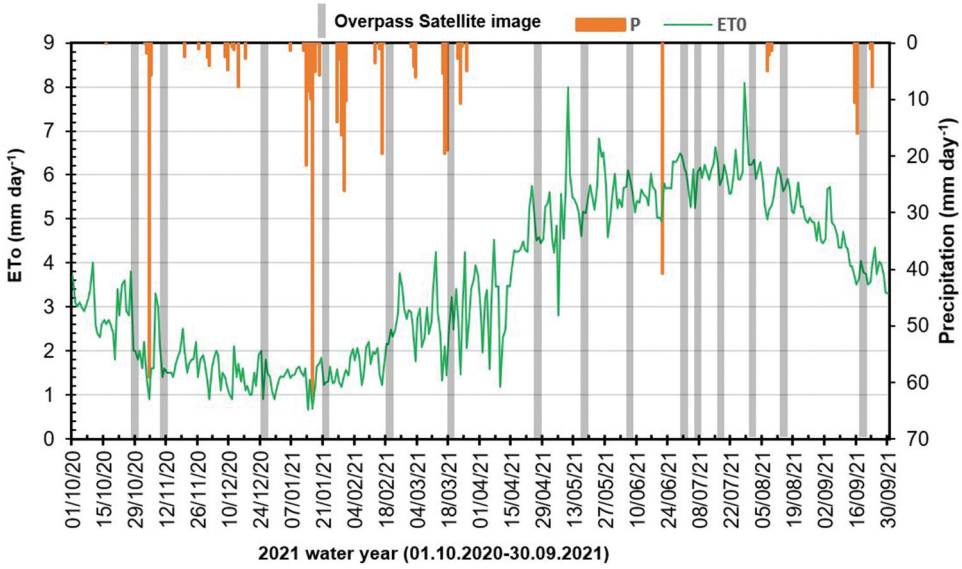


Figure 4. Temporal variability of observed daily precipitation (P, mm) and calculated daily reference evapotranspiration (ETo, mm) values during the 2021 water year in the irrigation sub-catchment located in the Lower Seyhan Plain, Turkey. Meteorological data were observed at the Cotlu station shown in Fig. 1. Vertical bars indicate the satellite overpass dates.

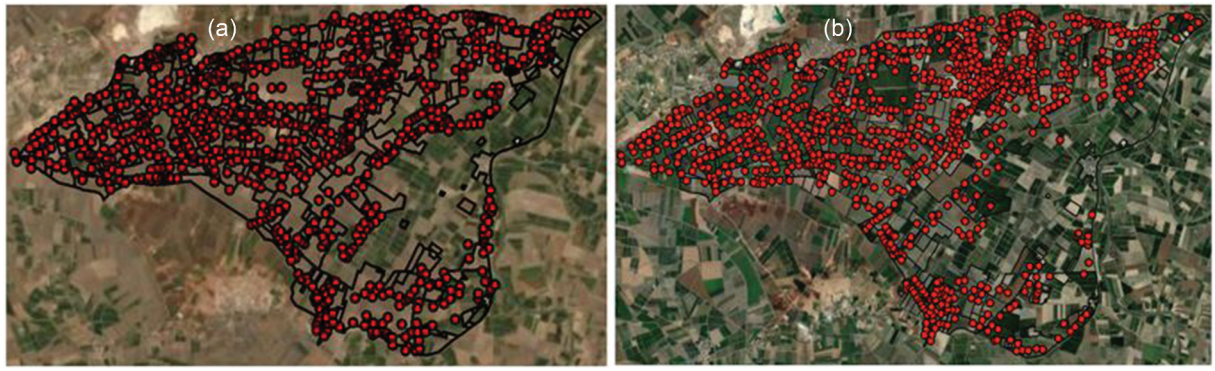


Figure 5. Locations visited for collecting ground truth data of various crops: (a) in winter and (b) in summer.

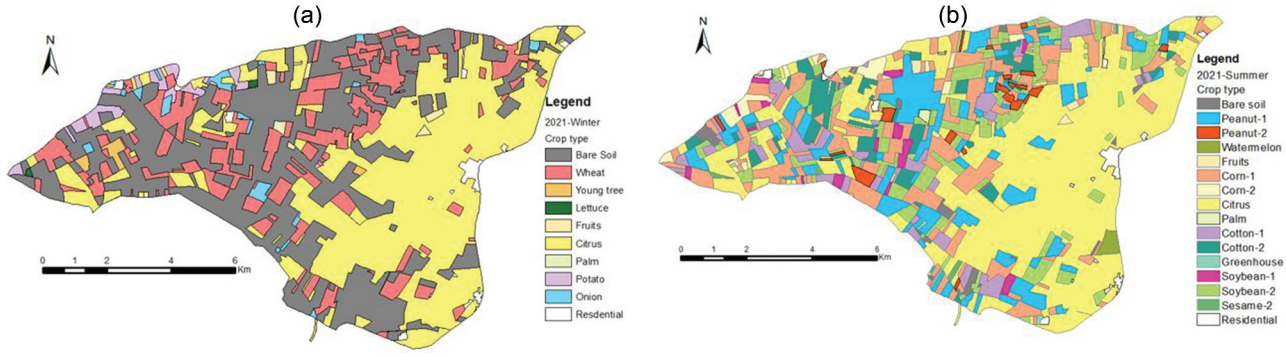


Figure 6. Distribution of crop types over the study area: (a) in winter and (b) in summer.

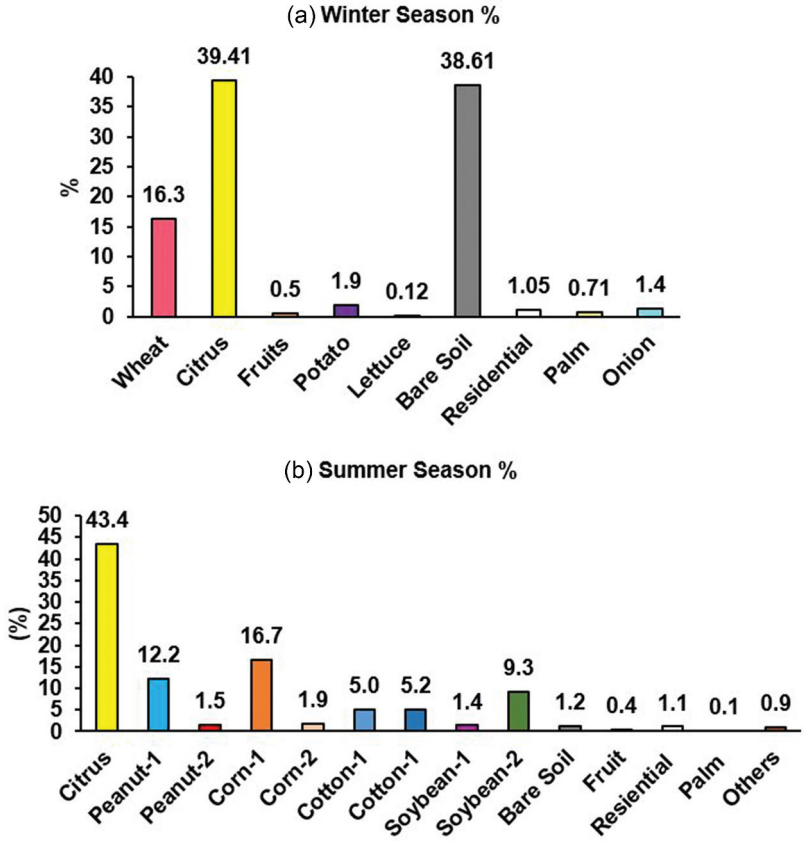


Figure 7. The percentage of area covered by different plants cultivated in the research area in the winter and summer seasons of the 2021 water year.

Table 4. Confusion matrix of the crop classification in the winter season. Figures stand for the number of parcels visited during the field campaigns.

		Ground reference crop									
Estimated crop	Class	Bare soil	Wheat	Lettuce	Fruit	Citrus	Palm	Potato	Onion	Total	%
	Bare soil	**341**	11	0	0	12	0	0	0	364	94
	Wheat	14	**184**	0	0	7	0	0	0	205	90
	Lettuce	0	0	**2**	0	0	0	0	0	2	100
	Fruit	1	0	0	**7**	4	0	0	0	12	58
	Citrus	17	0	0	0	**215**	0	0	0	232	93
	Palm	0	0	0	0	0	**1**	0	0	1	100
	Potato	0	0	0	0	0	0	**27**	0	27	100
	Onion	2	0	0	0	0	0	0	**23**	25	92
	Total	375	195	2	7	238	1	27	23	**868**	–

first crop planting in the summer season. In contrast, corn as the first (Corn-1) and second (Corn-2) crop was the most common crop (18.6% in total) in the summer season. The bar charts in Fig. 7(a) and (b) provide detailed information on the percentage of crop types by summer and winter seasons.

When the testing data were implemented using the ANN algorithm in the ENVI software, a confusion matrix was obtained for the winter and summer seasons. In this regard, Tables 4 and 5 show the number of fields that are classified and confused with another crop by the ANN model. As shown in Table 4, the overall accuracy percentage (between ground reference crop and estimated crop) was calculated for the crops grown in the winter season. It is clear that some of the crops such as lettuce and potato achieved 100% estimation accuracy; others, such as bare soil, wheat, citrus, and onion, achieved accuracy values of more than 90%. To put it another way, fields where onion and wheat were grown did not achieve a perfect classification accuracy (i.e., 100%). Ground truth data were collected in the first week of March 2021. At that time, we observed that wheat and onion crops partially covered the land surface. Therefore, it is highly probable that these plants were confused with the bare soil. In contrast, the accuracy of fruit fields was 58.0%; they were confused with citrus trees (33.3%) and fallow lands (8.3%). This type of confusion may be due to the deciduous fruit trees, such as apple, pomegranate, peach, etc., and the very young citrus saplings having more or less similar land features of bare soil in winter.

Similarly, a confusion matrix was obtained for crop fields in the summer season (Table 5). As shown in Table 5, some of the crops were classified without ever being confused with others (Sesame-2, palm, and watermelon), i.e., 100% classification accuracy. In contrast, other crops have been classified with an accuracy of more than 77%, except for fruit trees. It can be explained that fruit trees have the highest confusion with citrus trees (43%) owing to their similar shape formation or coverage features. The accuracy results of ANN classification showed us that the ANN model in the ENVI program misclassified fruit trees as young citrus samplings, resulting in low estimation accuracy. However, the crop-based classification accuracy of ANN technology has resulted in accuracies higher than 85% for the preponderant crops grown in the study area, such as wheat, citrus, corn, cotton, etc.

3.3 Spatial variability of energy balance (EB) components and ETa by the METRIC model

In this study, METRIC-based actual evapotranspiration, i.e., ETa-METRIC (hereafter, ETa), estimates were acquired using Landsat satellite images and instantaneous local meteorological data observed in L8 and Cotlu stations in the Lower Seyhan Plain located in the Eastern Mediterranean Region of Turkey. To this end, energy balance (EB) components of each image were derived seriatim. For example, Fig. 8 illustrates EB components (latent heat, net radiation, soil heat flux, sensible heat flux) on DOY 198 as an example. In this paper, we used the R-METRIC model, which has automatized hot–cold pixel selection that decreases the possibility of human error (Aksu and Arikan 2017).

The mean values of EB components estimated by the METRIC model at the time of the satellite overpass are presented in Table 6. In addition, the table includes the mean surface temperature and the G/Rn ratio. As shown in Table 6, G/Rn ratios ranged from 0.14 to 0.26 during the satellite images overpass. Generally, the ratio of G to R_n varies based on vegetation cover, soil moisture, and the time of observation (Kustas *et al.* 1993). For example, Ramírez-Cuesta *et al.* (2018) found the mean ratio of G to R_n to be 0.16 at the time of satellite overpass when using Landsat satellite images, indicating that the G/Rn ratios acquired for the day of the image overpass are consistent with the literature.

Finally, ETa for the day of the image overpass was calculated using Equation (13) on a pixel basis, and areal mean values were obtained at the time of the satellite overpass. Accordingly, Fig. 9 shows the temporal variations of areal mean ETa values over the study area. The annual total ETa was found to be about 1254.5 mm, and the daily mean, maximum, and minimum ETa were estimated as 3.44, 6.97, and 0.99 mm day^{-1}, respectively. Figure 10 illustrates temporal variations of monthly ETa over the study area: the highest value of ETa (163 mm) was estimated in July, while the lowest value (68 mm) was obtained in January. In terms of crop types and growing seasons, high ETa values occurred in the mid-season, corresponding to the peak IS, i.e., July, whereas low ETa rates occurred in the early and late growing seasons (Fig. 10). As stated clearly by Senay *et al.* (2016), this variation in ETa might be due to different land use/land cover types, vegetation growing periods, and growth stages, climate, and soil moisture availability.

ETa maps reflected the changes in parallel with crop type variations and spatial coverage of crops over the study area on DOY 22 and DOY 198 (Fig. 11). On DOY 22, citrus was the highest value (2.16 mm day^{-1}) of mean ETa-METRIC, while potato was the lowest value (1.55 mm day^{-1}) of mean ETa since potato crops are at the very early stage of stolon initiation during this period (Fig. 2). Likewise, on DOY 198, the

Table 5. Confusion matrix of the crop classification in the summer season. Figures stand for the number of parcels visited during the field campaigns.

		Ground reference crop															
Estimated crop	Class	Citrus	Corn-2	Corn-1	Cotton-1	Peanut-1	Soybean-2	Cotton-2	Bare soil	Sesame-2	Soybean-1	Peanut-2	Fruit	Palm	Watermelon	Total	%
	Citrus	**194**	0	1	0	1	0	0	0	0	0	0	0	0	0	196	99
	Corn-2	0	**25**	1	0	0	0	0	0	0	0	0	1	0	0	26	86
	Corn-1	13	1	**192**	3	5	7	1	0	0	0	0	3	0	0	226	85
	Cotton-1	0	0	2	**65**	0	2	4	0	0	0	0	0	0	0	74	88
	Peanut-1	9	0	5	0	**114**	3	0	0	0	0	1	1	0	0	133	86
	Soybean-2	1	0	6	0	0	**111**	2	1	0	1	0	0	0	0	122	91
	Cotton-2	3	0	2	1	0	0	**68**	0	0	0	0	0	0	0	74	92
	Bare soil	2	0	3	0	0	0	0	**22**	0	0	0	0	0	0	28	79
	Sesame-2	0	0	0	0	0	0	0	0	**3**	0	0	0	0	0	3	100
	Soybean-1	1	0	0	0	0	4	0	0	0	**21**	0	0	0	0	26	81
	Peanut-2	2	0	3	0	0	1	2	0	0	0	**27**	0	0	0	35	77
	Fruit	3	0	0	0	0	0	0	0	0	0	0	**3**	1	0	7	43
	Palm	0	0	0	0	0	0	0	0	0	0	0	0	**1**	0	1	100
	Watermelon	0	0	0	0	0	0	0	0	0	0	0	0	0	**1**	**1**	100
	Total	229	26	216	69	120	128	77	23	3	22	28	8	2	**1**	**952**	–

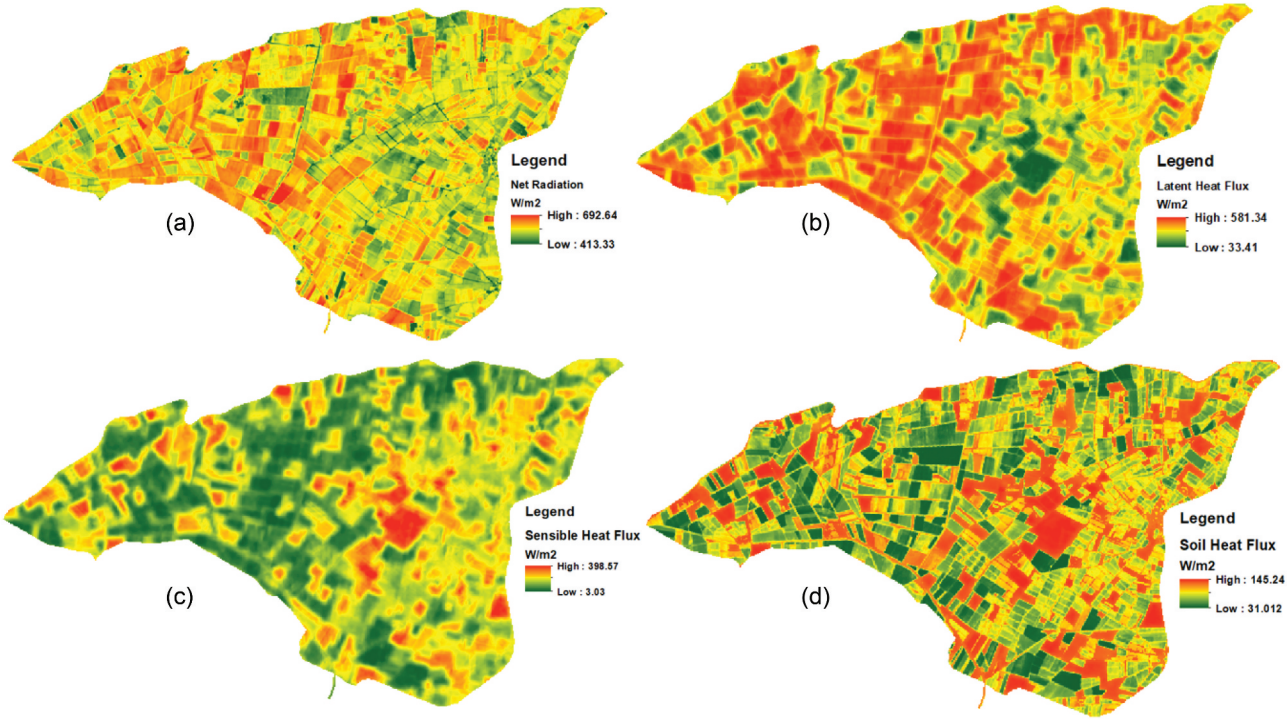


Figure 8. Spatial distribution of remote sensing-derived energy balance (EB) components over the irrigated catchment on DOY 198: (a) net radiation (Rn), (b) latent heat flux (LE), (c) sensible heat flux (H), and (d) soil heat flux (G) in W m^{-2}.

Table 6. Temporal variation of average energy balance (EB) components and surface temperature estimated by the METRIC model over the study area in the 2021 water year (from 26 October 2020 to 19 September 2021).

EB\date	DOY 300	DOY 316	DOY 364	DOY 22	DOY 54	DOY 79	DOY 118	DOY 134	DOY 158	DOY 182	DOY 190	DOY 198	DOY 214	DOY 230	DOY 262
Rn (W m^{-2})	360.17	323.59	256.31	351.20	450.91	473.12	609.79	629.41	556.20	616.53	521.87	603.74	584.06	545.73	513.42
G (W m^{-2})	93.58	77.80	58.1	51.48	68.23	77.98	101.16	103.64	109.03	95.24	95.50	87.17	84.83	82.66	77.76
H (W m^{-2})	53.71	3.32	−21.31	90.56	78.99	54.77	225.47	222.48	74.42	161.70	14.33	149.99	93.73	128.29	125.99
LE (W m^{-2})	212.87	242.47	219.52	209.17	303.69	340.38	283.23	303.29	372.74	359.59	412.04	366.58	405.51	334.79	309.67
Ts (K)	312.55	305.77	297.56	284.66	293.29	302.34	308.48	312.65	319.61	314.66	316.90	312.83	314.07	310.00	307.39
G/Rn	0.26	0.24	0.23	0.15	0.15	0.16	0.17	0.16	0.20	0.15	0.18	0.14	0.15	0.15	0.15
LE+H (W m^{-2})	266.59	245.80	198.21	299.72	382.68	395.15	508.70	525.77	447.17	521.29	426.37	516.57	499.24	463.08	435.66
Rn-G (W m^{-2})	266.59	245.80	198.21	299.72	382.68	395.14	508.62	525.77	447.17	521.29	426.37	516.57	499.24	463.08	435.66

maximum value of mean ETa (6.31 mm day^{-1}) was determined for the first crop corn (corn-1), since water and nutrients are in high demand to meet growth needs; and watermelon had the minimum value of mean ETa (1.91 mm day^{-1}). Both cotton-1 and soybean-1 had a similar value of mean ETa (6.24 mm day^{-1}) on DOY 198.

Temporal variations of areal mean ETa values for each crop type are presented in Fig. 12 during the overpass satellite images in the winter season. On both DOY 300 and DOY 316, remarkably low values of mean ETa were recorded for wheat. In the same context, the mean ETa value for wheat increased sharply from 1.98 mm day^{-1} on DOY 22 to 3.98 mm day^{-1} on DOY 54, then gradually increased to reach the highest value of 4.7 mm day^{-1} on DOY 118. Potato had a similar behaviour in terms of the temporal variations of mean ETa. The mean values of ETa, however, were less than those of wheat crop. ETa values of lettuce were the lowest on the last three dates compared to other crop types (wheat, potato, and citrus), showing a good agreement with the growing stages of the crops. Concordantly, areal mean actual evapotranspiration values for citrus were the highest on 29 December in 2020, and 22 January in 2021, compared to other crops. Similarly, ETa for wheat was higher than that of potato and lettuce on both DOY 54 and DOY 79.

Figure 13 congruently illustrates the changes in areal mean ETa values of some specific crops at the time of the Landsat satellite overpass during the summer season. In this regard, the areal mean ETa for Corn-1 reached its highest level (6.91 mm day^{-1}) on DOY 182; then it

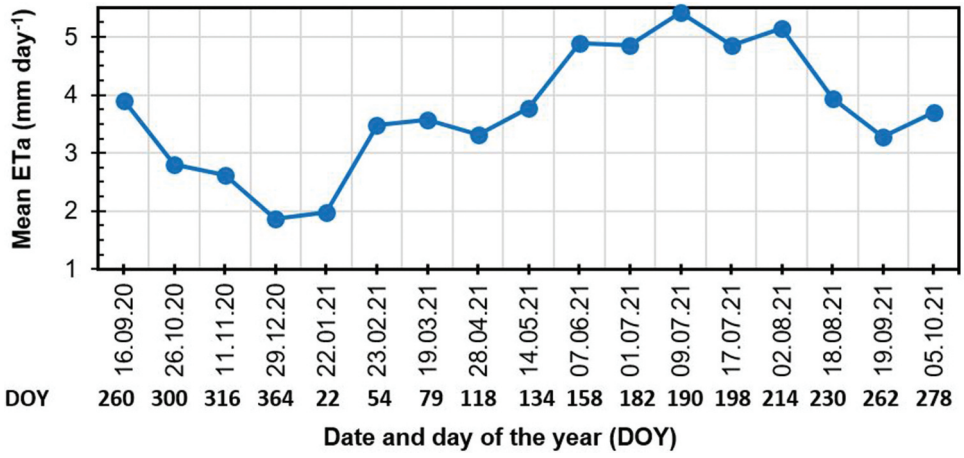


Figure 9. Temporal variations of areal mean daily ETa values, acquired by the METRIC approach, at the time of satellite overpass over the study area.

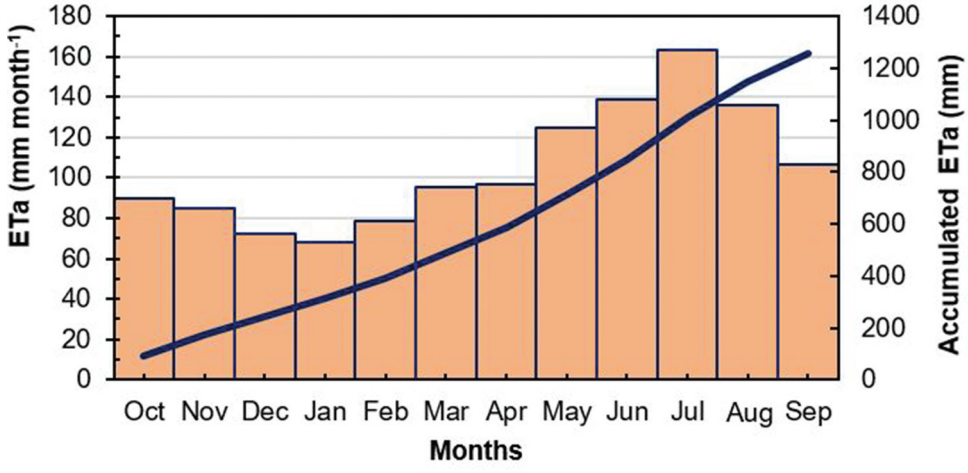


Figure 10. Changes in actual evapotranspiration (ETa) values by month for the 2021 hydrological year.

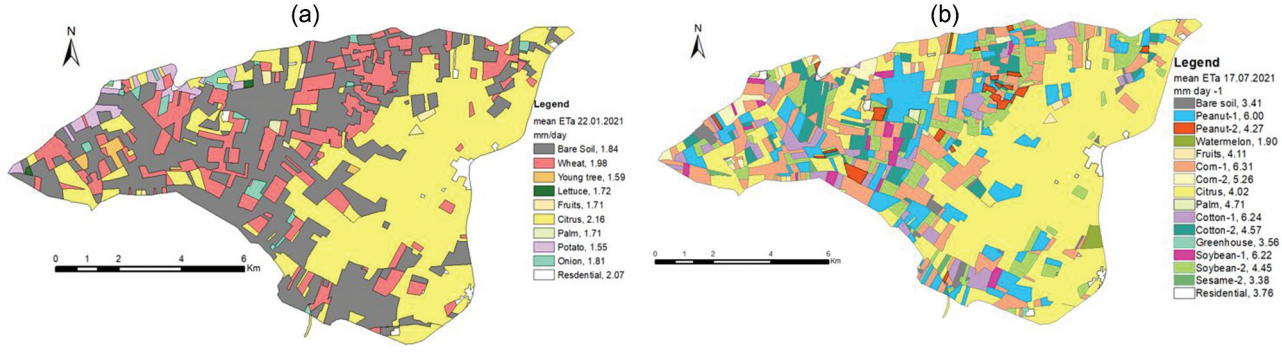


Figure 11. Spatial and temporal variations of the plant-based averages of actual evapotranspiration values (ETa, mm day^{-1}), acquired by METRIC, over the irrigated catchment in two extreme cases: (a) rainy condition on DOY 22; and (b) heavy irrigation application during an extreme drought period, on DOY 198.

decreased remarkably and reached its lowest value (3.41 mm day^{-1}) on DOY 230 (since corn-1 is almost at the harvesting stage at that time). Citrus ETa values varied between 3.26 and 4.75 mm day^{-1}, indicating a decreasing temporal trend behaviour; ETa for soybean-2 and peanut-1 showed more or less similar behaviour. However, areal mean ETa values of peanut-1 were generally higher than those for soybean-2 as shown in Fig. 13.

3.4 Temporal variations of water balance components at the catchment level

Water balance components were measured at all irrigation and drainage gauging stations as shown in Fig. 1. However, annual and monthly evapotranspiration (ETa and ETc) values were estimated by employing the METRIC model and the "two-step procedure" at the catchment level in the 2021 water year. Then, we calculated the change in catchment storage (both in the

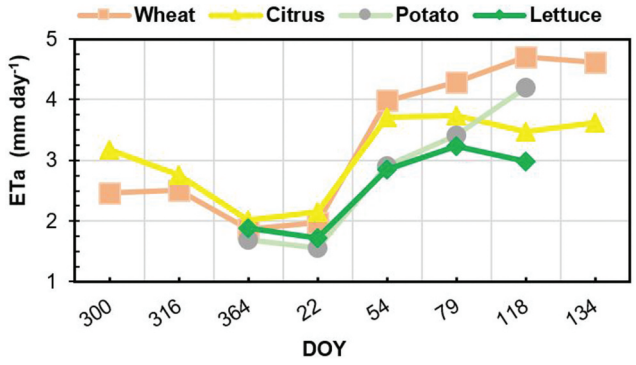


Figure 12. Temporal variations in areal mean ETa (mm day^{-1}) values of winter crops at the time of satellite overpass.

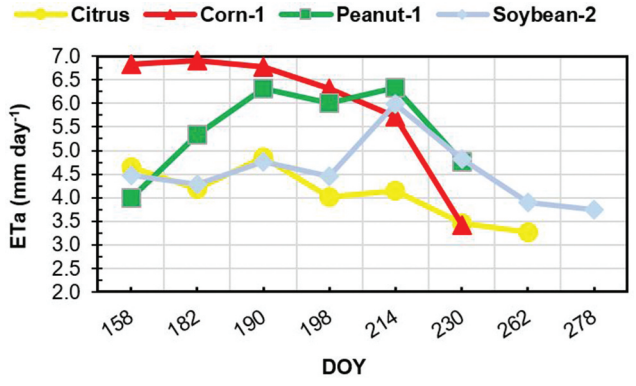


Figure 13. Temporal variability of areal mean ETa-METRIC (mm day^{-1}) estimates for summer crops, commonly grown in the study site, during the overpass satellite images in the summer.

vadose zone, i.e., rooting depth, and in the water table), based on the ETa estimated by the METRIC model, precipitation, and net drainage, i.e., IRFs and irrigation diversions were measured daily at the gauging stations using automatic water level recorders with a measurement precision of ±1.0 mm.

It should be emphasized that there is no exact technique for measuring the amount of water stored in the rooting depth and shallow water body at the catchment level in a given period due to the fuzziness, complexity, stochasticity, and uncertainty in the hydrologic system. Therefore, in this study, the change in the catchment storage was termed a closure error of the hydrologic water balance work, i.e., ±ΔS. Water balance results are given in Table 7 for the 2021 water year. As shown in Table 7, the closure error term calculated in Equation (4), ΔS, helped us to emphasize that seven or more consecutive months of water deficit, particularly in the winter season, except for January (108 mm) may occur in the research area. However, surplus water is always available at the catchment in June, July, August, and September, including the peak IS. The annual change in ΔS was about +67.08 mm, showing surplus water in the yearly period, with an incurred error of 3.34% (Table 7; Figs 14 and 15).

Figure 15 summarises the values of yearly water balance components in the 2021 water year. It can be seen from Fig. 15 that annual actual evaporation and IRFs, i.e., drainage, are 1254.5 and 719.0 mm, respectively. However, the annual drainage (719.0 mm) of the catchment is surprisingly greater than precipitation (476.6 mm), resulting in an unexpectedly high annual runoff coefficient of 1.50 as compared to the Seyhan River Basin (0.53) of which our study area is a part, and compared to the Eastern Black Sea Basin which has the highest runoff coefficient (0.72) in Turkey (Cetin 2020b). The high value of the annual runoff coefficient should be attributed to irrigation water diversions to the AID and anthropogenic activities such as drainage and irrigation practices in dry periods. In conclusion, the resulting high runoff coefficient constitutes substantial evidence of inefficient use of irrigation water at the catchment. Furthermore, although the "Error Δ" in Table 7 is subject to remarkable changes by month, it was about 7.62% in the IS, but 15.43% in the non-IS. Ibrikci *et al.* (2015) pointed out that mass balance components at the catchment level are subject to measurement uncertainties and errors; consequently, an error of less than 20% is considered "low" and acceptable.

3.5 Comparison of ETa by the METRIC model with ETc method

The areal mean ETa values of each crop on the satellite image acquisition dates were compared with the ETc of that crop (Allen *et al.* 1998). To this end, three crop types were selected for comparison: wheat, potato, and lettuce in the winter; corn-1, peanut-1, soybean-2 in the summer; and citrus for the whole year.

Table 7. In-situ measurement results of inflow and outflow components of the general hydrologic water balance model, change in the system, and quantified closure errors by month at the catchment level.

Months	Drainage (Q or IRFs, mm)	Irrigation (I, mm)	Precipitation (P, mm)	Pef	METRIC-ETa (mm)	ΔS (mm)	Error Δ (%)
October	88.6	146.0	0.0	0.0	89.7	−32.26	−19.89
November	72.3	77.9	73.0	33.8	84.6	−6.04	−3.92
December	29.5	1.0	23.8	4.3	72.0	−76.73	−121.41
January	29.0	16.9	189.0	126.2	68.0	108.87	71.86
February	37.7	22.5	25.0	5.0	78.7	−68.86	−84.08
March	55.2	53.2	56.2	23.7	95.1	−40.97	−31.55
April	78.0	92.8	51.8	21.1	96.5	−30.02	−18.81
May	92.0	215.5	0.8	0.0	124.7	−0.52	−0.24
June	77.3	300.7	0.0	0.0	138.8	84.60	32.74
July	64.0	288.1	0.0	0.0	163.5	60.62	23.51
August	56.8	227.3	10.4	0.0	135.9	45.01	20.91
September	38.5	122.1	46.6	18.0	106.9	23.37	14.88
Total (yearly)	**719.0**	**1564.0**	**476.6**	**232.0**	**1254.5**	**67.08**	**3.34**

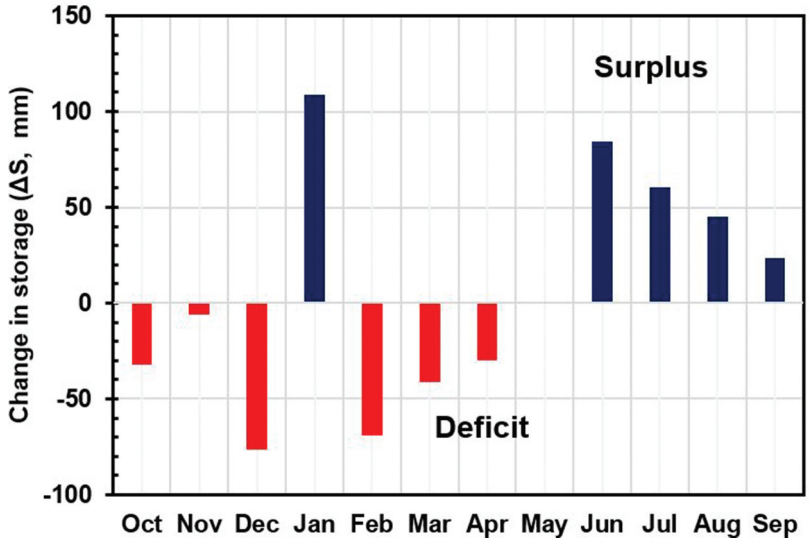


Figure 14. Monthly changes of catchment storage in the root zone (vadose zone) and/or shallow water table in the 2021 water year.

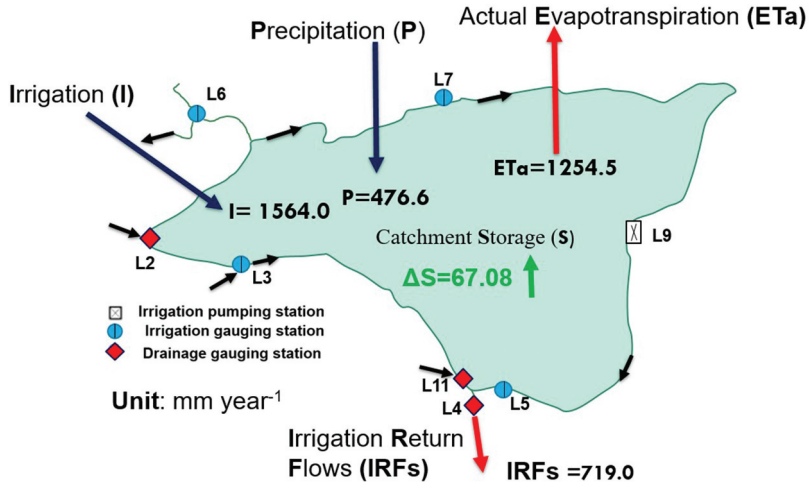


Figure 15. Water balance components in the 2021 water year.

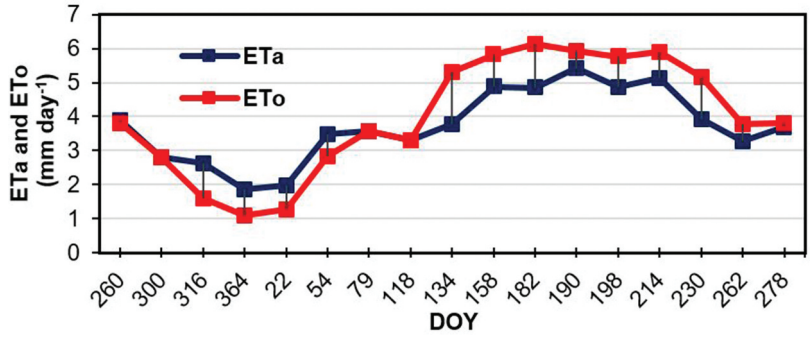


Figure 16. Temporal variations of actual evapotranspiration acquired from ETa and reference evapotranspiration (ETo) derived from the FAO-56 model at the time of the Landsat satellite overpass.

3.5.1 Comparison of ETa with ETc method for satellite image acquisition dates

ETo values calculated by the FAO-Penman-Monteith method and ETa values generated by METRIC in the study area are presented in Fig. 16 during the satellite images overpass. The values of ETa were higher than the values of ETo in the winter season, indicating that ET_rF_i values (in Equation 15), viz. corresponding to the Kc value in Equation (2), are greater than 1.0. This fraction can be interpreted that METRIC-derived ETa takes into account all the climate variables, soil, and plant types together. In contrast, ETo was higher than ETa in the summer season. Similarly, Fig. 17 shows the same

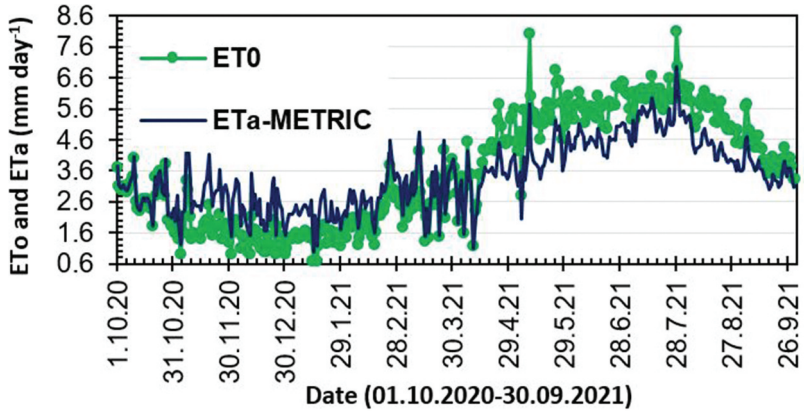


Figure 17. Temporal variations of METRIC ETa, interpolated for the days between satellite images by employing Equations (13) and (14), and ETo for the 2021 water year.

variation of ETa with ETo for the whole 2021 water year. The annual ETo (1308.0 mm) was higher than ETa (1254.5 mm). The annual ETc from the study area as a whole is equal to about 71% of ETa, indicating that Kc values for the crop development stages in ETc method are generally lower than ET_rF_i fraction in ETa estimation.

Comparisons between the estimated ETa and calculated ETc values were carried out for some crop types during the growing seasons at the times of satellite overpass. Furthermore, to evaluate the estimation capability of the METRIC procedure, daily areal mean estimation results of ETa were further evaluated for some specific crop types by comparing them with independently estimated ET values (Tasumi 2019) following the FAO-56 "two-step procedure" (hereafter, ETc) as given in Allen *et al.* (1998). To this end, daily ETc series were firstly derived by considering crop types and growing stages in the AID for satellite image acquisition dates in both the winter and summer seasons; then, ETc and ETa values acquired for wheat, potato, lettuce, corn-1, peanut-1, soybean-2, and citrus were presented in Fig. 18. The values of ETa are surprisingly close to the ETc values for the wheat, and the difference between ETa and ETc ranged from 0.32 to 1.78 mm day^{-1}. Also, the values of ETa are very close to the values of ETc in potato, lettuce, corn-1, peanut-1, and soybean-2. Results on some dates matched exactly, as shown in Fig. 18.

In addition, Fig. 18 illustrates the mean variation of the ETc method compared with ETa for citrus for the whole year. During this period, the estimated ETa for the citrus-planted areas was, to some extent, higher than ETc for the same crop. The difference might be due to the selection of Kc values (standard Kc) from the available literature by TAGEM-DSI (2017) based on the phenological cycle of citrus. Put another way, ETc calculations do not consider stressed conditions like the METRIC model does, and the ETc procedure does not consider evaporation from the bare soil. A simple linear relationship between ETa and ETc values of some crop types grown in the winter and summer seasons is shown in Fig. 19, and the results showed a good agreement between the two types of estimation. Table 8 shows a summary of the statistical analysis between ETa and ETc. The simple linear regression analyses applied by many other researchers showed a good relationship between the ETa-METRIC and direct methods like lysimeter (Allen *et al.* 2007a), the eddy covariance method (Liebert *et al.* 2016), and Bowen energy ratio (Carrasco-Benavides *et al.* 2014), among others. Allen *et al.* (2007b) summarized the results of 19 studies that include verification of results from METRIC and/or SEBAL, and only 4.5% disagreement was reported on average.

In addition, many studies have applied direct methods to estimate ETa in the Cukurova region where our study area is located. One of the studies was applied to estimate ETa by lysimeter for soybean-2 and compare it with PySEBAL. The R^2 was 0.73, and the value of ETa by lysimeter was 4.4 mm day^{-1} on 28 September in 2009 (Sawadogo *et al.* 2020), while ETa by METRIC was 4.73 mm day^{-1} in 2021. Moreover, we estimated ETa using METRIC for soybean-2 in the pixel as shown in Fig. 20 and compared it with lysimeter and pySEBAL on 16 July (in 2009) and 1 August (in 2009). The black pixel represents the lysimeter field which is located in the centre of the 0.12 ha field at the Research Fields of the Agricultural Structures and Irrigation Department, Faculty of Agriculture, University of Cukurova (37°1′N, 35°21′E; 20 m above sea level), Adana, Turkey, as shown in Fig. 20. Based on these results, the value of the ETa-METRIC was 2.53 mm day^{-1} on DOY 197 (16 July 2009) and 2.81 mm day^{-1} on DOY 213 (1 August 2009), while the ETa obtained by the lysimeter was 2.9 and 2.5 mm day^{-1} for the same two dates, respectively.

Similarly, Sawadogo *et al.* (2020) found that the value of the ETa calculated by the pySEBAL in the same pixel was 2.3 and 3.1 mm day^{-1} for DOY 197 and DOY 213, respectively. The values of ETa obtained by the METRIC model were very close to the lysimeter measurements as compared to the pySEBAL for soybean-2 in 2009. Madugundu *et al.* (2017) did research on an irrigated field in Saudi Arabia and reported a high correlation between ETa by the METRIC and eddy covariance method (R^2 = 0.93). Additionally, the METRIC model was applied in Idaho and compared with lysimeter measurements (Allen *et al.* 2005). Those authors obtained an error in evapotranspiration of 4% for lawn and 1% for sugar beet in the plant growing season. Likewise, in-situ water balance closure errors (in Table 7), and hence changes in catchment storage, increased remarkably

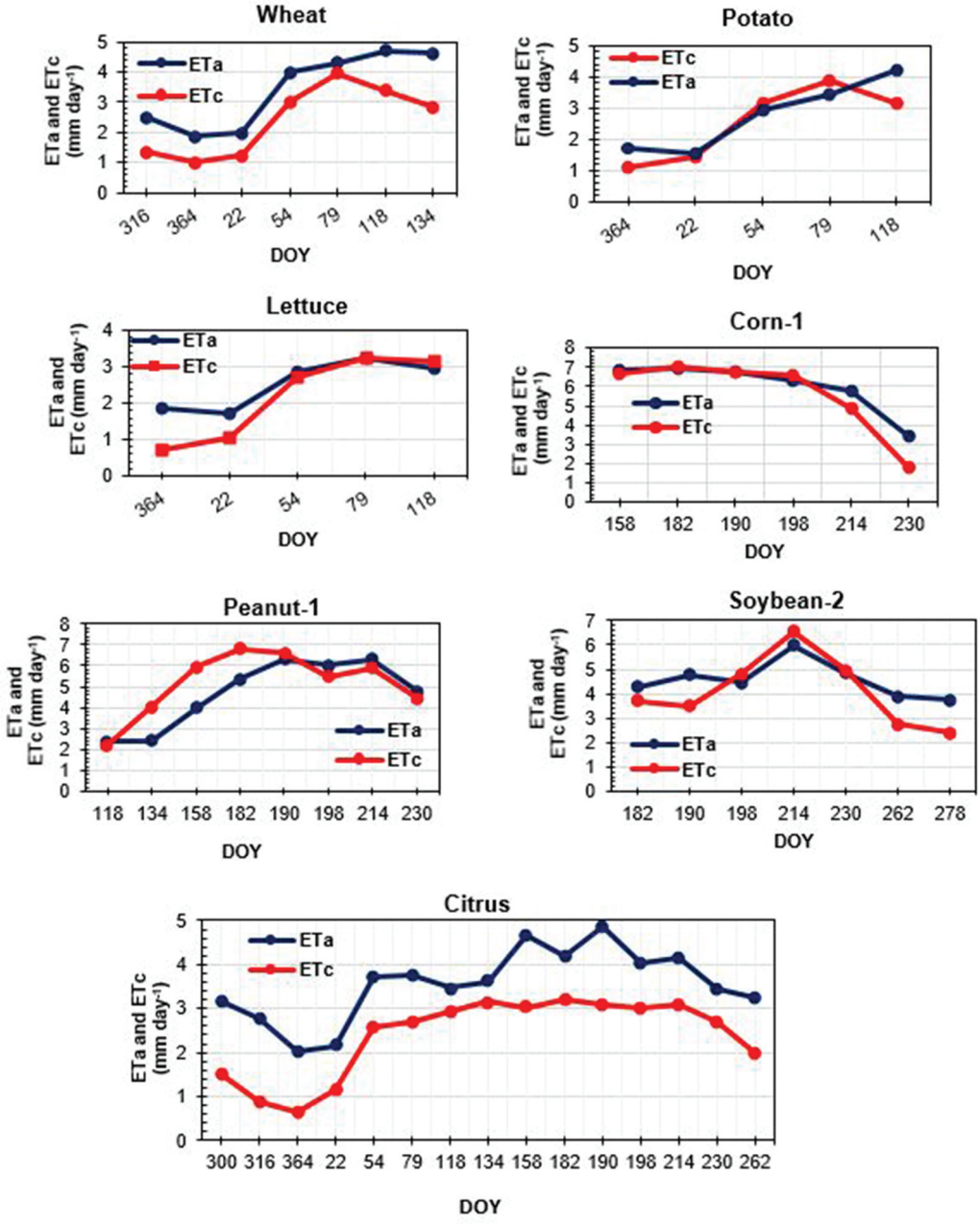


Figure 18. Evolution of ETa and ETc values of different crop types across the satellite image acquisition dates.

when using ETc compared to using ETa. Consequently, in-situ water balance closure errors indicate that the METRIC model might be a useful tool for irrigation managers as well as farmers to estimate actual evapotranspiration rates in large-scale irrigation catchments, and METRIC-ETa values are superior to the independently estimated ETc values acquired by FAO-56.

3.5.2 Comparison of ETa from the METRIC model with ETc method for the monthly and seasonal time scale

Figure 21 shows monthly ETa and ETc values estimated for the winter crops (wheat, potato, and lettuce) and summer crops (corn-1, peanut-1, and soybean-2) grown in the 2021 hydrological year, and for citrus grown year round. The seasonal ETa and ETc series showed more or less similar temporal patterns. Seasonal ETa values (741, 387, and 371 mm) were higher than the seasonal ETc values (489, 329, and 329 mm) for wheat, potato, and lettuce, respectively. The seasonal ETa values (893 and 529 mm) were slightly higher than the seasonal ETc (841 and 503 mm) for corn-1 and soybean-2, respectively, while the seasonal ETc value (755 mm) was higher than ETa (691 mm) for peanut-1.

The results showed that there was a slight difference between the seasonal ETa derived from METRIC and the ETc method. This difference might be due to the selection of Kc by growth stages, growing lengths and periods, and non-homogeneities in planting/sowing dates of field crops. For example, previous studies applied direct methods to estimate ETa for some crop types in the study area. One of them was

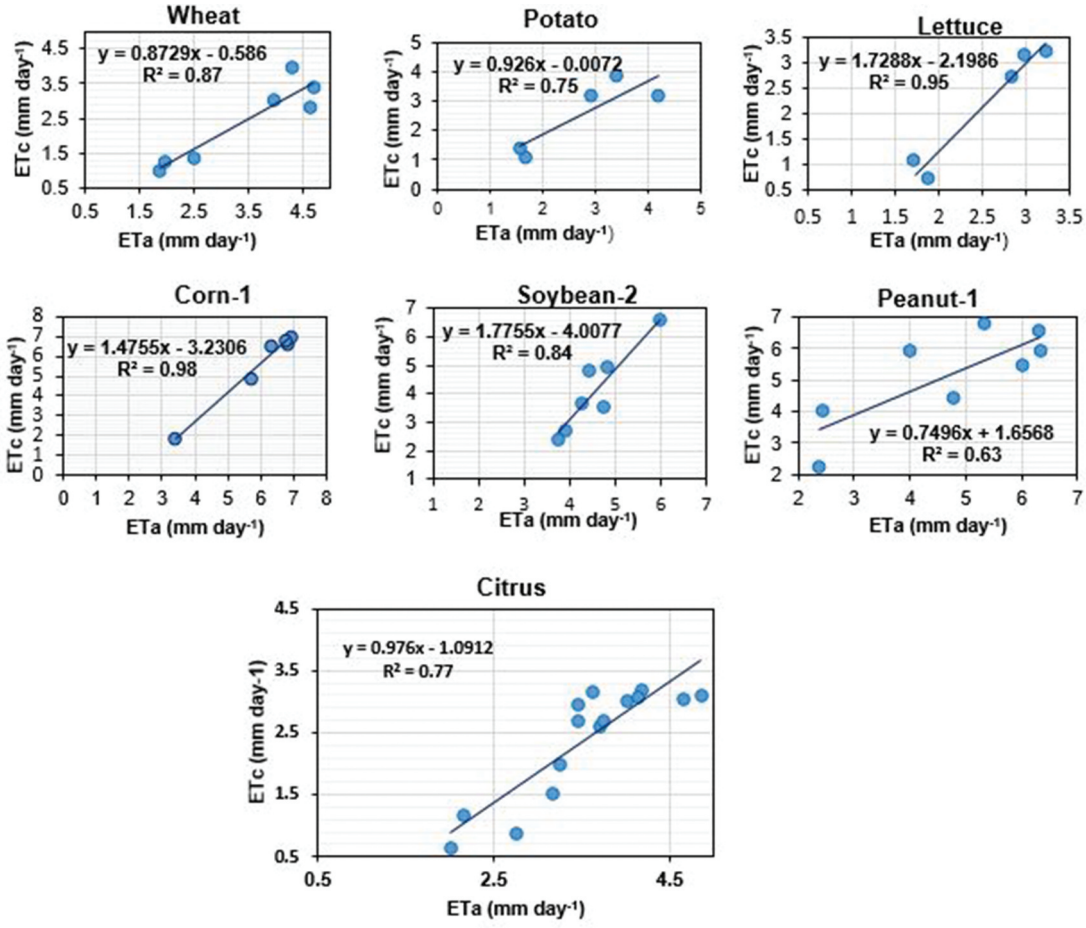


Figure 19. The linear relationship between FAO-56 ETc and METRIC ETa for some crop types commonly grown in the catchment.

Table 8. Performance statistics of ETa-METRIC and ETc for some crops.

	RMSE (mm day^{-1})	MBE (mm day^{-1})	R^2
Wheat	1.11	1.02	0.87
Potato	0.59	0.21	0.75
Lettuce	0.61	0.35	0.95
Corn-1	0.74	0.38	0.98
Soybean-2	0.89	0.47	0.84
Peanut-1	1.07	−0.48	0.63
Citrus	1.25	1.18	0.77

used to estimate ETa for soybean-2 in 2009. In the same context, the seasonal cumulative ETa from the lysimeter for soybean-2 was 354 mm from (25 June 2009 to 6 October 2009), whereas the Bowen ratio–energy balance (BREB) totals were 405 mm (Unlu *et al.* 2010). In contrast, the seasonal cumulative ETa from the METRIC for the same period (25 June to 6 October) of soybean-2 was found to be 491 mm. However, we applied the METRIC model in the 2021 hydrological year, so the ETa value in this study was higher than in the previous studies due to the inherent spatiotemporal variability in evapotranspiration. In addition, the ongoing climate change impact during the last decade might be another reason for this difference (Selek *et al.* 2016). Another study estimated ETa for wheat in 2003–2004 in the same region as our study area; the seasonal evapotranspiration of wheat under irrigated conditions was calculated as 708 mm using the water balance method (Koc and Kanber 2020), while the seasonal

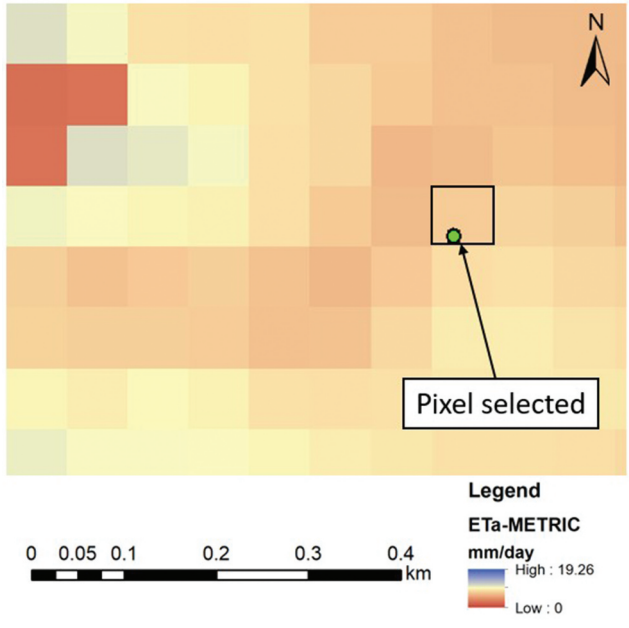


Figure 20. ETa-METRIC map for soybean-2 on 16 July 2009.

evapotranspiration of wheat by the METRIC model was 711 mm in the winter season of 2021, indicating a good approximation in the estimation of actual evapotranspiration.

The METRIC model can produce detailed information on energy balance components as a spatial and temporal

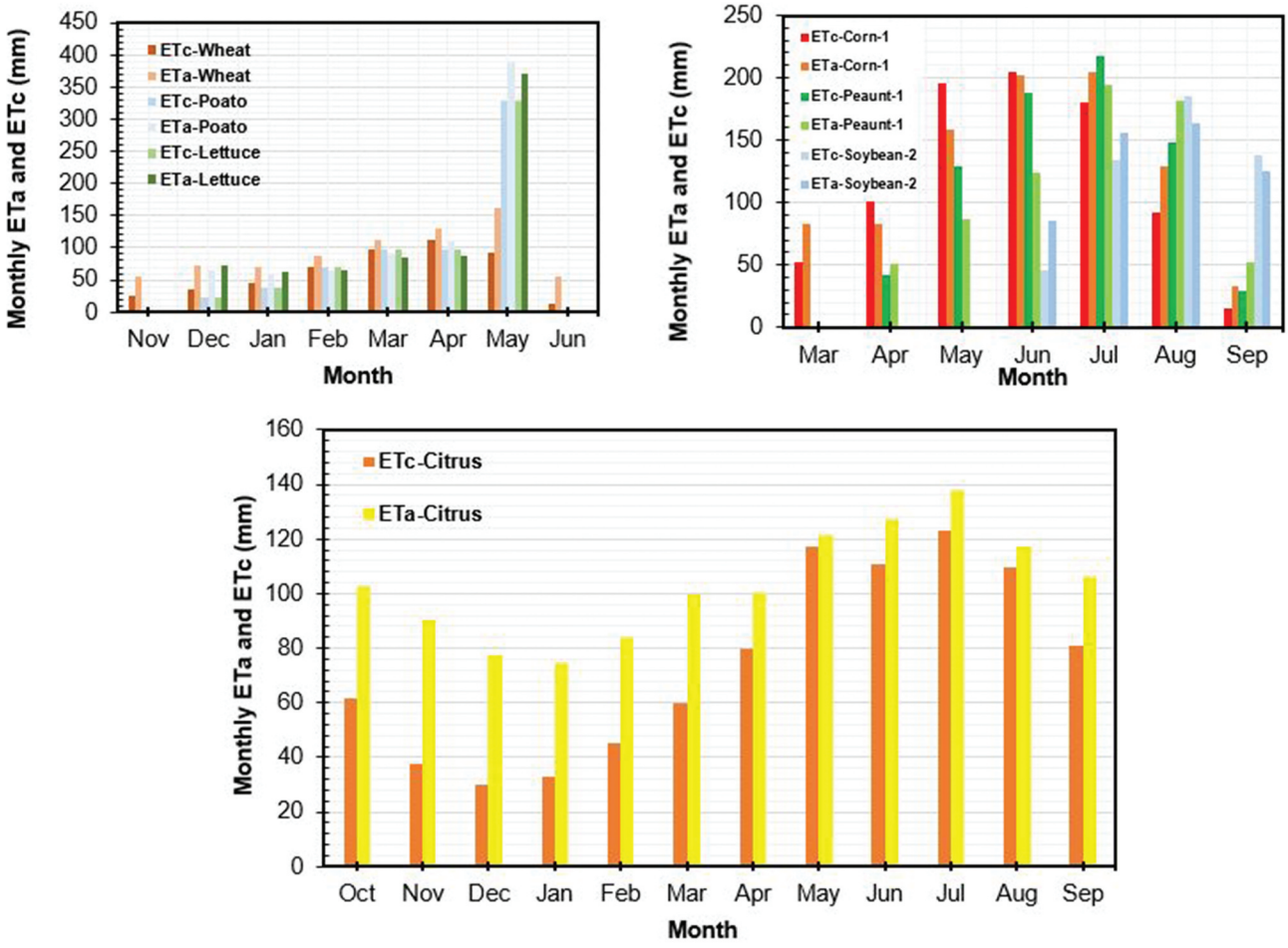


Figure 21. Variability in plant-based METRIC ETa and FAO-56 ETc values by month.

distribution (Fig. 8). This information can be used as a test tool for further analysis such as a comparison of available energy for evapotranspiration and measured ET values (Aksu and Arikan 2017). In addition, energy fluxes are a useful by-product of the METRIC model. Therefore, METRIC-estimated energy balance (EB) components can be used to estimate some agronomic indexes, such as the crop water stress index (Sun *et al.* 2004), and some components of the water balance model. In this regard, based on the areal mean evapotranspiration calculations for specific crops, the METRIC algorithm shows good performance in estimating ETa for large irrigation schemes with a variety of cropping patterns in the Mediterranean Basin of Turkey. The overall assessment of results – and of the water balance closure errors in particular – led us to conclude that the METRIC model is superior to the ETc approach and produces more reliable results at the catchment scale.

4 Conclusions

This research was carried out in a catchment with large-scale irrigation located in a semi-arid region (a) to quantify components of basic hydrologic water budget equation by realizing in-situ flow measurements of water in and out of the catchment, (b) to estimate actual evapotranspiration (ETa) from RS images and ETc by the "two-step approach," (c) to classify crop types with an artificial neural network (ANN) using data of high spatial resolution, and finally (d) to demonstrate the representativeness of ETa estimates in a catchment with large-scale irrigation by comparing it with water budget closure errors. Studies on in-situ observations of water balance components and ETa comparisons with water balance closure errors are not very common. Hence, the novelty of this study lies in the scarcity of similar research both in our study area and in other semi-arid regions of the world. Moreover, in-situ measurements of precipitation and runoff rates at the outlet of the catchment enabled us to calculate the annual runoff coefficient to assess how efficiently irrigation water has been utilized by the farmers. In turn, the annual runoff coefficient was found to be extremely high (1.50) compared to that of the natural river basins. Evaluating the annual runoff coefficient in large-scale irrigation schemes is critical to understanding the hydrological cycle under both natural and anthropogenic changes and can provide valuable information to decision-makers and water managers for managing water resources by the optimal method.

Classifying crop types by ANN using satellite data of high spatial resolution resulted in a high level of accuracy – over 92%. Provided that the hydrometric measurement network is available in the basin, the methodology proposed in the current study can be used to estimate ETa basinwide and

to perform crop classification with an ANN algorithm in forming water balances to minimize the measurement errors incurred in large-scale irrigation districts similar to our study area.

The results obtained from the METRIC model, viz. ETa, and ETc were used as an input to the water balance work and helped us to elaborate on the method for assessing water balance closure errors at the catchment scale. Image analysis results from employing the ANN algorithm were found to be in good agreement with ground truth data and demonstrated that citrus plantations were predominant in the winter and summer seasons of the 2021 water year, at 39.4% and 43.4%, respectively. Bare soils, i.e., fallow areas, made up 38.61% of the study area in the winter, while first-crop corn (Corn-1) constituted nearly 17% of the study area in the summer. The annual total ETo, ETa, and ETc values were calculated as 1308, 1255, and 890 mm, respectively, in the 2021 water year. However, there is a good agreement between ETa and ETc values for the crops of wheat, potato, lettuce, corn-1, peanut-1, soybean-2, and citrus in both the winter and summer seasons. Furthermore, the METRIC results showed a good agreement with the ETc of crops.

The spatial and temporal variation of ETa maps is driven mainly by land use, meteorological conditions, and vegetation crop patterns. ETa maps produced by the METRIC model reflected changes that occurred in parallel with crop type variations over the study area in the winter and summer seasons of 2021. The annual change in the catchment storage was surplus water with a value of +67.08 mm and an estimated error of 3.34%. Although the closure error is subject to remarkable changes from one month to another, it was about 7.62% in the IS but 15.43% in the non-IS, indicating that water balance closure errors are low and acceptable for practical applications.

In this regard, the use of ETa values in forming water balances resulted in smaller water balance closing errors compared to ETc usage. Smaller closing errors of in-situ water balance work are interpreted as indicative of the acceptable estimation performance of the satellite-based METRIC algorithm for actual evapotranspiration estimation in the irrigated Mediterranean landscapes. Therefore, the ETa maps from RS can be used as input data for a better understanding of agricultural hydrology and managing agricultural water at the catchment level. In addition, it may be concluded that the METRIC algorithm is a potentially appropriate tool to evaluate actual evapotranspiration, and the outcome can be used as a basis for planning and management of agricultural catchments located in the arid and semi-arid regions of the world. Provided that crop types are determined precisely by adapting a dependable technology like the ANN used in this study, crop-based ETa values can be reliably estimated for a better allocation of freshwater resources in a basin. Therefore, this research can be expanded in future by comparing the spatial-temporal variability of actual crop evapotranspiration (ETa) and crop coefficient (Kc) with model simulations (past and future). It can also be used to evaluate how climate change will affect crop evapotranspiration in drought-prone regions in the 21st century.

Acknowledgements

The authors thank the Turkish National Geodesy and Geophysics Union (TUJJB).

Disclosure statement

No potential conflict of interest was reported by the authors.

Funding

This work was supported by the Turkish National Geodesy and Geophysics Union (TUJJB) [TUJJB-TUMEHAP-2020-01]. Additionally, this work was partially supported by the Scientific Research Projects (BAP) Coordination Unit of Cukurova University [Project Number: FBA-2019-11309].

ORCID

Mahmut Cetin http://orcid.org/0000-0001-5751-0958
Omar Alsenjar http://orcid.org/0000-0001-9471-794X
Hakan Aksu http://orcid.org/0000-0003-4686-7446
Muhammet Said Golpinar http://orcid.org/0000-0002-3536-4563
Mehmet Ali Akgul http://orcid.org/0000-0002-5517-9576

References

Aksu, H., and Arikan, A., 2017. Satellite-based estimation of actual evapotranspiration in the Buyuk Menders Bain, Turkey. *Hydrology Research*, 48 (2), 559–570. doi:10.2166/nh.2016.226

Allen, R.G., et al., 1998. Crop evapotranspiration – guidelines for computing crop water requirements. FAO Irrigation and Drainage Paper 56, Rome, Italy, FAO.

Allen, R.G., et al., 2007b. Satellite-based energy balance for mapping evapotranspiration with internalized calibration, METRIC (applications). *Journal of Irrigation and Drainage Engineering*, 133, 395–406. doi:10.1061/(ASCE)0733-9437(2007)133:4(395)

Allen, R.G., et al., 2011a. Satellite-based ET estimation in agriculture using SEBAL and METRIC. *Hydrological Processes*, 25, 4011–4027. doi:10.1002/hyp.8408

Allen, R.G., et al., 2011b. Evapotranspiration information reporting: I. Factors governing measurement accuracy. *Agricultural Water Management*, 98, 899–920. doi:10.1016/j.agwat.2010.12.015

Allen, R.G., et al., 2013. Sensitivity of landsat-scale energy balance to aerodynamic variability in mountains and complex terrain. *JAWRA Journal of the American Water Resources Association*, 49 (3), 592–604. doi:10.1111/jawr.12055

Allen, R.G., Tasumi, M., and Morse, A., 2005. Satellite-based evapotranspiration by METRIC and Landsat for western states water management. US Bureau of reclamation evapotranspiration workshop, Alaska, USA, 8–10.

Allen, R.G., Tasumi, M., and Trezza, R., 2007a. Satellite-based energy balance for mapping evapotranspiration with internalized calibration, METRIC (model). *Journal of Irrigation and Drainage Engineering*, 133, 380–394. doi:10.1061/(ASCE)0733-9437(2007)133:4(380)

Anderson, M.C., et al., 2012. Remote sensing of environment use of landsat thermal imagery in monitoring evapotranspiration and managing water resources. *Remote Sensing of Environment*, 122, 50–65. doi:10.1016/j.rse.2011.08.025

Bastiaanssen, W.G.M., et al., 1998a. A remote sensing surface energy balance algorithm for land (SEBAL): 1. *Journal of Hydrology*, 212–213, 198–212. doi:10.1016/S0022-1694(98)00253-4

Bastiaanssen, W.G.M., et al., 1998b. A surface energy balance algorithm for land (SEBAL): 2. Validation. *Journal of Hydrology*, 212–213, 213–229. doi:10.1016/S0022-1694(98)00254-6

Belgiu, M., and Csillik, O., 2018. Remote sensing of environment Sentinel-2 cropland mapping using pixel-based and object-based time-weighted

dynamic time warping analysis. *Remote Sensing of Environment*, 204, 509–523. doi:10.1016/j.rse.2017.10.005

Biggs, T.W., Marshall, M., and Messina, A., 2016. Mapping daily and seasonal evapotranspiration from irrigated crops using global climate grids and satellite imagery: automation and methods comparison. *Water Resources Research*, 52, 7311–7326. doi:10.1002/2016WR019107

Boken, V.K., et al., 2004. Agricultural water use estimation using geospatial modeling and a geographic information system. *Agricultural Water Management*, 67 (3), 185–199. doi:10.1016/j.agwat.2004.01.003

Carrasco-Benavides, M., et al., 2014. Parameterization of the satellite-based model (METRIC) for the estimation of instantaneous surface energy balance components over a drip-irrigated vineyard. *Remote Sensing*, 6 (11), 11342–11371. doi:10.3390/rs61111342

Cetin, M., et al., 2020a. Analysis of irrigation performance in water resources planning and management: a case study. *Fresenius Environmental Bulletin (FEB)*, 29 (5), 3409–3414.

Cetin, M., 2020b. Agricultural water use. In: N.B. Harmancioglu and D. Altinbilek, eds. *Water resources of Turkey, world water resources*. Vol. 2. Cham, Switzerland: Springer Nature, 257–302. doi:10.1007/978-3-030-11729-0_9

Courault, D., Seguin, B., and Olioso, A., 2005. Review on estimation of evapotranspiration from remote sensing data: from empirical to numerical modeling approaches. *Irrigation and Drainage Systems*, 19, 223–249. doi:10.1007/s10795-005-5186-0

Daly, C., et al., 2008. Physiographically sensitive mapping of climatological temperature and precipitation across the conterminous United States. *International Journal of Climatology*, 28 (15), 2031–2064. doi:10.1002/joc.1688

Defourny, P., et al., 2019. Near real-time agriculture monitoring at national scale at parcel resolution: performance assessment of the Sen2-Agri automated system in various cropping systems around the world. *Remote Sensing of Environment*, 221, 551–568. doi:10.1016/j.rse.2018.11.007

Gowda, P.H., et al., 2008. ET mapping for agricultural water management: present status and challenges. *Irrigation Science*, 26 (3), 223–237. doi:10.1007/s00271-007-0088-6

He, R., et al., 2017. Evapotranspiration estimate over an almond orchard using Landsat satellite observations. *Remote Sensing*, 9 (5), 436. doi:10.3390/rs9050436

Hirich, A., Choukr-Allah, R., and Ragab, R., 2020. *Emerging research in alternative crops*. Environment & Policy. Switzerland: Springer Nature, 376.

Ibrikci, H., et al., 2015. Irrigation-induced nitrate losses assessed in a Mediterranean irrigation district. *Agricultural Water Management*, 148, 223–231. doi:10.1016/j.agwat.2014.10.007

Jaafar, H.H., and Ahmad, F.A., 2020. Remote sensing of environment time series trends of landsat-based ET using automated calibration in METRIC and SEBAL : the Bekaa Valley, Lebanon. *Remote Sensing of Environment*, 244, 1. doi:10.1016/j.rse.2018.12.033

Jiang, Y., et al., 2020. Large-scale and high-resolution crop mapping in China using sentinel-2 satellite imagery. *Agriculture*, 10, 433. doi:10.3390/agriculture10100433

Karnez, E., 2010. *Evaluation of nitrogen budget inputs and outputs in wheat and corn growing areas in lower*. Thesis (PhD). Çukurova University, Institute of Natural and Applied Sciences, Soil Science and Plant Nutrition. (In Turkish).

Koc, D.L., and Kanber, R., 2020. Determination of evapotranspiration for wheat by using bowen ratio energy balance method. *KSU Tarim ve Doga Dergisi*, 3 (2), 544–553. (In Turkish). doi:10.18016/ksutarimdoga.vi.597980

Kustas, W.P., Daughtry, C.S.T., and Van Oevelen, P.J., 1993. Analytical treatment of the relationships between soil heat flux/net radiation ratio and vegetation indices. *Remote Sensing of Environment*, 46 (93), 319–330. doi:10.1016/0034-4257(93)90052-Y

Landerer, F.W., and Swenson, S.C., 2012. Accuracy of scaled GRACE terrestrial water storage estimates. *Water Resources Research*, 48, W04531. doi:10.1029/2011WR011453

Liebert, R., et al., 2016. Reduced evapotranspiration from leaf beetle induced tamarisk defoliation in the Lower Virgin River using satellite-based energy balance. *Ecohydrology*, 9 (1), 179–193. doi:10.1002/eco.1623

Loucks, D.P., and Van Beek, E., 2005. Water resources systems planning and management. *Studies and Reports in Hydrology*, 1–680. UNESCO.

Madugundu, R., et al., 2017. Performance of the METRIC model in estimating evapotranspiration fluxes over an irrigated field in Saudi Arabia using Landsat-8 images. *Hydrology and Earth System Sciences; Katlenburg-Lindau*, 21 (12). doi:10.5194/hess-21-6135-2017

Mahlayeye, M., Darvishzadeh, R., and Nelson, A., 2022. Cropping patterns of annual crops: a remote sensing review. *Remote Sensing*, 14, 2404. doi:10.3390/rs14102404

Mokhtari, A., et al., 2021. Actual evapotranspiration from UAV images : a multi-sensor data fusion actual evapotranspiration from UAV images : a multi-sensor data fusion approach. *Remote Sensing*, 13 (12), 2315. doi:10.3390/rs13122315

Novelli, A., et al., 2016. Improving the ANN classification accuracy of landsat data through spectral indices and linear transformations (PCA and TCT) aimed at LU/LC monitoring of a river basin. In: *Computational science and its applications – ICCSA 2016. ICCSA 2016. Lecture notes in computer science*. Vol. 9787, 420–432. Cham: Springer, doi:10.1007/978-3-319-42108-7_32

Numata, I., et al., 2017. Evaluation of landsat-based METRIC modeling to provide high-spatial resolution evapotranspiration estimates for amazonian forests. *Remote Sensing*, 9, 46. doi:10.3390/rs9010046

Olmedo, G.F., Ortega-farias, S., and Fonseca-luengo, D., 2016. Tools and functions to estimate actual evapotranspiration using land water : tools and functions to estimate actual evapotranspiration using land surface energy balance models. *The R Journal*, 8, 352. doi:10.32614/RJ-2016-051

Ozcan, H., Cetin, M., and Diker, K., 2003. Monitoring and assessment of land use status by GIS. *Environmental Monitoring and Assessment*, 87, 33–45. doi:10.1023/A:1024433812336

Ramírez-Cuesta, J.M., et al., 2018. Impact of the spatial resolution on the energy balance components on an open canopy olive orchard. *The International Journal of Applied Earth Observation and Geoinformation*, 74, 88–102. doi:10.1016/j.jag.2018.09.001

Rouse, J.W., et al., 1974. Monitoring the vernal advancement and retrogradation (Greenwave effect) of natural vegetation. Final Rep. RSC 1978-4, Santana, R.C., Barros, N.F., Leite, H.G, Remote Sensing Center. Texas A&M Univ., College Station.

Sawadogo, A., et al., 2020. Comparative analysis of the pySEBAL model and lysimeter for estimating actual evapotranspiration of the soybean crop in Adana. *International Journal of Engineering and Geosciences (IJEG)*, 5 (2), 60–65. Turkey. doi:10.26833/ijeg.573503

Selek, B., et al., 2016. Seyhan Dam, Turkey, and climate change adaptation strategies. Chapter 10 in increasing resilience to climate variability and change. In: C. Tortajada, ed. *Water resources development and management*. Springer Science Business Media Singapore, 205–226. doi:10.1007/978-981-10-1914-2_10

Senay, G.B., et al., 2016. Evaluating Landsat 8 evapotranspiration for water use mapping in the Colorado River Basin. *Remote Sensing of Environment*, 185, 171–185. doi:10.1016/j.rse.2015.12.043

Sonobe, R., et al., 2017. Assessing the suitability of data from Sentinel-1A and 2A for crop classification. *GIScience & Remote Sensing*, 54, 6, 918–938. doi:10.1080/15481603.2017.1351149

Steduto, P., 2000. Plant nutrient management under pressurized irrigation systems in the Mediterranean Region: crop water requirements. In: J. Ryan, ed. *Plant nutrient management under pressurized irrigation systems in the Mediterranean Region. Proceedings of the International Fertigation Workshop organized by the World Phosphate Institute (IMPHOS)*, 25–27 April 1999. Aleppo: ICARDA, 400

Su, Z., 2002. The surface energy balance system (SEBS) for estimation of turbulent heat fluxes. *Hydrology and Earth System Sciences*, 6, 85–100. doi:10.5194/hess-6-85-2002

Sun, J.F., et al., 2004. Air temperature retrieval from remote sensing data based on thermodynamics. *Theoretical and Applied Climatology*, 80, 37–48.

Swenson, S., and Wahr, J., 2006. Post-processing removal of correlated errors in GRACE data. *Geophysical Research Letters*, 33, L08402. doi:10.1029/2005GL025285

TAGEM-DSI, 2017. *Plant water consumption of irrigated plants in Turkiye*. Ankara, Turkiye: The Republic of Turkiye, Ministry of Agriculture and Forestry, General Directorates of Agricultural Research and Policies (TAGEM) and State Hydraulic Works (DSI), Published by TAGEM. 590. (In Turkish).

Tapley, B.D., et al., 2004a. The gravity recovery and climate experiment: mission overview and early results. *Geophysical Research Letters*, 31, L09607. doi:10.1029/2004GL019920

Tasumi, M., 2003. *Progress in operational estimation of regional evapotranspiration using satellite imagery*. Ph.D. thesis. University of Idaho.

Tasumi, M., 2019. Estimating evapotranspiration using METRIC model and Landsat data for better understandings of regional hydrology in the western Urmia Lake Basin. *Agricultural Water Management*, 226 (2019), 105805. doi:10.1016/j.agwat.2019.105805

Trezza, R., Allen, R.G., and Tasumi, M., 2013. Estimation of actual evapotranspiration alongthe Middle Rio Grande of New Mexico using MODIS and Landsat imagery with the METRIC model. *Remote Sensing*, 5 (10), 5397–5423. doi:10.3390/rs5105397

Unlu, M., Kanber, R., and Kapur, B., 2010. Comparison of soybean evapotranspiration measured by weighing lysimeter and Bowen ratio-energy balance methods. *African Journal of Biotechnology*, 9 (30), 4700–4713.

Whyte, A., Ferentinos, K.P., and Petropoulos, G.P., 2018. A new synergistic approach for monitoring wetlands using Sentinels −1 and 2 data with object-based machine learning algorithms. *Environmental Modelling and Software*, 104, 40–54. doi:10.1016/j.envsoft.2018.01.023

Zalnezhad, A., et al., 2022. Comparing performance of ANN and SVM methods for regional flood frequency analysis in South-East Australia. *Water*, 14, 3323. doi:10.3390/w14203323

Zheng, B., et al., 2015. International journal of applied earth observation and geoinformation a support vector machine to identify irrigated crop types using time-series Landsat NDVI data. *The International Journal of Applied Earth Observation and Geoinformation*, 34, 103–112.